The solubility of La hydroxide and stability of La^{3+} and La hydroxyl complexes at acidic to mildly acidic pH from 25 to 250 °C

Kevin Padilla [1,2,*], Alexander P. Gysi [1,2]

[1] Department of Earth and Environmental Science, New Mexico Institute of Mining and Technology, 801 Leroy Place, Socorro, NM 87801, USA

[2] New Mexico Bureau of Geology and Mineral Resources, New Mexico Institute of Mining and Technology, 801 Leroy Place, Socorro, NM 87801, USA

* Corresponding author: endykevin.padillarivas@student.nmt.edu

Tel: +1 575-835-5754

REVISION 1

To be submitted to GCA, *for the Special Issue "Hydrothermal Geochemistry and Beyond: A Tribute to Terry M. Seward"*

Keywords: *rare earth elements; solubility; hydrothermal; speciation; thermodynamics*

Abstract

The mobility of rare earth elements (REE) in natural hydrothermal systems can be assessed using geochemical modeling, which requires reliable thermodynamic data of relevant aqueous species. In this study, we evaluate the controls of pH and temperature on La speciation and the role of hydroxyl complexes in REE transport at hydrothermal conditions. Batch-type hydrothermal solubility experiments were conducted using synthetic La hydroxide powders equilibrated in perchloric acid-based aqueous solutions at temperatures between 150 and 250 °C and starting pH of 2 to 5. The La hydroxide solubility is retrograde with temperature and displays a strong pH dependence with a decrease in La concentrations from acidic to mildly acidic pH spanning between 3 to 5 orders of magnitude (e.g. log La molality of -2.5 to -7.2 at 250 °C). Thermodynamic optimizations using GEMSFITS allow to retrieve the standard partial molal Gibbs energies for the La^{3+} aqua ion and the formation constants for the La hydroxyl species (i.e., $LaOH^{2+}$, $La(OH)_2^{+}$, $La(OH)_3^{0}$) between 25 and 250 °C. A comparison between the experimentally derived thermodynamic properties with the calculated values from the Helgeson-Kirkham-Flowers equation of state parameters indicates an increased divergence with temperature. Discrepancies in standard partial molal Gibbs energies range between ~1−12 kJ/mol and result in a predicted La hydroxide solubility differing by up to 3 orders of magnitude at 250 °C. Speciation calculations indicate a higher stability of La^{3+} and $LaOH^{2+}$ over the other La hydroxyl species in the studied pH range of 3.4 to 6. The optimized thermodynamic properties for La aqueous species have important implications for modeling the solubility of REE minerals such as monazite and the mobility of REE in hydrothermal systems.

1. INTRODUCTION

The rare earth elements (REE) are important strategic and critical metals used in a wide range of technologies (Hatch, 2012; Goodenough et al., 2018). In geologic systems, hydrothermal aqueous fluids play an important role in the formation of many REE mineral deposits as evidenced by the presence of hydrothermal veins containing REE minerals (Salvi and Williams-Jones, 1996, 2006; Williams-Jones et al., 2000; Smith et al., 2000, 2015; Cook et al., 2013; Moore et al., 2015; Gysi et al., 2016; Harlov et al., 2016; Vasyukova and Williams-Jones, 2019; Liu et al., 2020; Beland and Williams-Jones, 2021). Thermodynamic modeling and experimental studies have further constrained the importance of chloride, fluoride, and sulfate complexes in mobilizing REE in acidic fluids based on available thermodynamic properties for most of these species (Migdisov and Williams-Jones, 2008, 2014; Migdisov et al., 2009, 2016, 2019; Williams-Jones et al., 2012; Gysi and Williams-Jones, 2013). Other studies indicate the potential importance of REE hydroxyl and carbonate complexes in more alkaline fluids, but the thermodynamic properties for these species are not yet well constrained (Perry and Gysi, 2018; Gysi and Harlov, 2021; Louvel et al., 2022; Nisbet et al., 2022; Han and Gysi, 2024; Pan et al., 2024).

Thermodynamic data for calculating the stability of the REE^{3+} aqua ions and aqueous REE hydroxyl complexes in hydrothermal fluids are largely based on the work by Wood (1990), Haas et al. (1995), Shock and Helgeson (1988), and Shock et al. (1997). The thermodynamic properties for these REE complexes are generally predicted at high temperature and pressure from the Helgeson-Kirkham-Flowers (HKF) equation of state parameters (Helgeson et al., 1981; Shock and Helgeson, 1988; Tanger and Helgeson, 1988; Shock et al., 1992), which are compiled

in the study by Haas et al. (1995) and Shock et al. (1997). These properties were derived several decades ago but are still widely used in many geochemical modeling programs, commonly also referred to as slop98.dat database, which was originally implemented in the program SUPCRT92 (Johnson et al., 1992). However, the accuracy of this database needs to be improved because the formation constants for many REE aqueous complexes (Migdisov et al., 2009, 2016) and the solubility of REE phosphate (Pan et al., 2024) determined experimentally in more recent years indicate discrepancies that can reach over 2 orders of magnitude.

Experimental data for the REE hydroxyl complexes are scarce at high temperature. Monazite and xenotime solubility experiments conducted between 100 and 250 °C in pH 2 solutions (Gysi et al., 2015, 2018; Van Hoozen et al., 2020; Gysi and Harlov, 2021) were used to derive a set of optimized thermodynamic properties for the REE^{3+} and $REEOH^{2+}$ species (Pan et al., 2024). These indicate that the HKF parameters derived by Haas et al. (1995) do not accurately predict the experimental solubility data in this temperature range. Wood et al. (2002) conducted potentiometric experiments between 30 to 290 °C which indicate that the predominance of Nd hydroxyl complexes is overpredicted with respect to the stability of the Nd^{3+} aqua ion. Deberdt et al. (1998) evaluate the hydrolysis of La and Gd hydroxyl complexes based on hydroxide solubility experiments conducted between 40 and 150 °C at pH from 5 to 9.5 and come to a similar conclusion for the La^{3+} and Gd^{3+} aqua ions. Despite these few experimental efforts, thermodynamic data for many REE hydroxyl complexes are still lacking and the stability for these species seems to remain ambiguous in hydrothermal aqueous fluids (Migdisov et al., 2016).

In this study, La hydroxide batch-type solubility experiments were conducted at acidic to mildly acidic pH and at temperatures between 150 and 250 °C. The solubility data are compared to available literature data and used to derive values for the standard partial molal Gibbs energy of formation for the La^{3+} and La hydroxyl aqueous species using the optimization program GEMSFITS (Miron et al., 2015). Moreover, a new set of equilibrium constants was retrieved for the solubility of La hydroxide and the hydrolysis of La^{3+} as a function of temperature between 25 and 250 °C. This study is part of a series of experimental contributions aimed at building an internally consistent dataset that is integrated in the MINES thermodynamic database (Gysi et al., 2023) for more accurately modeling the nature and stability of REE aqueous species and assessing the mobility of REE in natural hydrothermal fluids.

2. MATERIALS AND METHODS

2.1. Materials

Lanthanum hydroxide powders were synthesized hydrothermally at 250 °C using a batch-type reactor (Parr 4744, Teflon-lined stainless steel) based on a method similar to Diakonov et al. (1998). The starting solution was prepared by mixing La_2O_3 powder (Alfa Aesar, REacton grade, 99.99% purity) with Milli-Q water (18 MΩ-cm). This solution was then transferred to the Teflon liner which was loaded in the reactor and purged using research grade nitrogen gas. The reactor was then placed into a preheated muffle furnace and allowed to equilibrate for three weeks. At the end of the synthesis procedure, the reactor was quenched in a water bath, and the mixture taken out of the reactor, filtered, and then oven dried at ~75 °C for at least 24 hours and stored in a desiccator. The solids were characterized using powder X-ray diffraction (XRD) analysis and

Rietveld refinement was carried out using the software MAUD (Lutterotti, 2000) adopting the hexagonal ($P6_3/m$) crystal system determined by Beall et al. (1977). The modeled and experimental spectra (Fig. 1) match the reference pattern of Beall et al. (1977) and the refined unit cell parameters are in agreement with those reported in the literature (Table 1). The La hydroxide solids synthesized have a purity of ~99% or better, which was verified by modeling a mixture of La hydroxide with other potential La phases (Fig. S1).

The perchloric acid-based experimental solutions were prepared by titrating appropriate amounts of perchloric acid (Fisher Scientific, trace metal grade) to 500 ml of Milli-Q water in order to reach a measured starting pH from 2 to 5 at room temperature. The pH was determined using a Metrohm 913 pH meter (precision of ± 0.003 pH units and resolution of 0.001 pH units) which was previously calibrated using Fisher Scientific pH buffers of 1.68, 4.01, and 7.0 (accuracy of 0.01). These pH values were then used to determine the starting molality of perchlorate (ClO_4^-) in the experimental solutions.

2.2. Experimental technique

Solubility experiments were performed using pure synthetic La hydroxide and perchloric acid-based solutions in 45 ml Teflon-lined stainless-steel batch-type reactors (Parr 4744) at temperatures of 150, 200, and 250 °C and at saturated water vapor pressure. The experimental technique is similar to the one used in previous REE phosphate solubility experiments (Gysi et al., 2018; Gysi and Harlov, 2021). The perchloric acid-based starting solutions used in the experiments have pH values of 2 to 5 in 0.5 pH unit increments. Perchloric acid was used because it can be assumed to be entirely dissociated in the studied temperature range (Migdisov

and Williams-Jones, 2007, 2008), and ClO_4^- does not readily complex with the REE (Choppin et al., 1966). These solutions were equilibrated at temperature with the La hydroxide powders for up to 10−14 days, with kinetic test experiments conducted between 1−26 days. Replicate experiments were conducted to determine the experimental uncertainty.

A schematic of the experimental design is shown in Fig. 2. A typical experiment consists of first loading each of the self-made Teflon sample holders (virgin grade purity) with ~40-50 mg of La hydroxide powder. These holders were then covered with Teflon tape, which was perforated using a 31-gauge needle and used as a permeable membrane to allow the experimental solutions and solid to react in the experiments; this membrane also slows down any back reaction upon quenching. The loaded sample holders were each placed into the Teflon-lined reactors which were each subsequently filled with 25 g of the perchloric acid-based starting pH buffer solutions. The reactor head space was purged with research grade nitrogen gas for 5 minutes, then rapidly closed and placed into a preheated muffle furnace (Cole-Palmer box furnace and Lindberg Blue M Thermo Scientific). The temperature was measured using a K-type thermocouple located in the center of the furnace and recorded with an Omega® temperature logger. The temperature was periodically examined during the experiments and maintained within ± 1 °C.

At the end of an experiment, the reactors were quenched in a cold water bath in less than 20 min and the solutions were extracted using a syringe and filtered using 0.22 μm membrane filters. The filtered experimental solutions were then acidified with HNO_3 (Fisher Scientific, trace metal grade) to avoid the formation of any precipitates. These acidified samples were further diluted and matrix matched with a 2% HNO_3 blank matrix solution. The diluted samples

were then analyzed for total dissolved La concentrations using inductively coupled plasma optical emission spectroscopy (ICP-OES) and quadrupole ICP mass spectrometry (ICP-MS).

The Teflon liners and sample holders were cleaned between experiments by applying an overnight acid wash using a ~10% sulfuric acid (Sigma-Aldrich, ACS reagent grade) solution and then soaked overnight with Milli-Q water. The Teflon sample holders were further cleaned using a CPX2800 Fisherbrand ultrasonic bath for 15 min. The acid washing solutions from the reactor were subsequently diluted and analyzed for La to test for any possible precipitates upon quenching. These test solutions displayed no detectable La concentrations using ICP-MS, and therefore, do not indicate any evidence of back reaction and precipitation of La on the reactor walls upon quenching.

2.3. Analytical method

The synthetic La hydroxide powders were characterized using a PANalytical X'Pert Pro XRD instrument with a Cu-Kα radiation source (1.541 Å wavelength) using 2θ scanning values ranging between 5° and 70° in 0.01° steps. Randomly oriented sample powders were mounted on (zero background) highly crystalline silicon single crystal plates. The measured diffractograms were background subtracted, the peak fitted and matched to the relevant phase identified using the X'Pert HighScore Plus software package.

Dissolved La concentrations were measured in acidified (2% HNO_3 matrix) samples using an Agilent 5900 ICP-OES, and samples with concentrations between 5 to 30 ppb were further analyzed using an Agilent 7900 quadrupole ICP-MS at the Analytical Chemistry Laboratory in the New Mexico Bureau of Geology and Mineral Resources, New Mexico Institute of Mining

and Technology. A series of diluted REE multi-standards (Inorganic Ventures, CMS-1, 10 ±0.04 ppm) were prepared for external calibration. Samples were spiked in-line with indium (SCP Science, NIST traceable) as an internal standard for drift corrections. For ICP-MS analysis, an in-line helium gas collision cell was used to reduce REE oxide formation. Individual La, Ce, Nd, and Eu standards (Inorganic Ventures, 1000 ±5 ppm) were prepared, and if necessary, used to correct for REE oxide formation using the same method as described by Gysi et al. (2018) and Aries et al. (2000). The analytical precision for ICP-OES analyses based on repeated standard measurements is better than 3% for standards measured in the concentration range of 30 to 1000 ppb La and the detection limit is 0.8 ppb La based on repeated analysis of the procedural blank (5σ). The analytical precision for ICP-MS analyses based on repeated standard analysis is better than 3% for La concentrations above 0.5 ppb and the detection limit is 7 ppt La based on 5σ of repeated blank analysis.

3. DATA TREATMENT

3.1. Aqueous speciation and pH calculations

Aqueous speciation and pH calculations were carried out using the GEMS code package (Kulik et al., 2013) and the MINES thermodynamic database (Gysi et al., 2023). The aqueous species considered in the calculations and the sources of thermodynamic data are listed in Table 2. The thermodynamic properties for La include the La^{3+} aqua ion reported by Shock and Helgeson (1988) and Shock et al. (1997) and the La hydroxyl complexes reported by Haas et al. (1995). The HKF parameters for these aqueous species implemented in the MINES database are originally from the slop98.dat thermodynamic dataset built-in the program SUPCRT92 (Johnson

et al., 1992), referred to hereafter as the Supcrt92 database. The properties for the La hydroxide solid are retrieved from the values reported by Diakonov et al. (1998) and Navrotsky et al. (2015) and presented in Table 3. These thermodynamic data for La hydroxide include the heat capacity function retrieved by Diakonov et al. (1998) based on calorimetric data from Chirico and Westrum (1980). This function is used to calculate the properties of the solid at the temperature of interest for initial equilibrium speciation and solubility calculations before thermodynamic parameter optimization (Section 3.2).

The TSolMod library (Wagner et al., 2012) is used in GEMS for all the activity and equation of state calculations. The thermodynamic properties of aqueous species are retrieved at the temperature and pressure of interest using the revised HKF equation-of-state (Helgeson et al., 1981; Shock and Helgeson, 1988; Tanger and Helgeson, 1988; Shock et al., 1992). The properties of H_2O are calculated from the IAPS-84 equation-of-state (Kestin et al., 1984). The activity coefficients (γ_i) of charged aqueous species are calculated using the extended Debye-Hückel equation:

$$log\gamma i = \frac{Az_i^2\sqrt{I}}{I + \mathring{a}B\sqrt{I}} + b_\gamma I \quad (1)$$

and the effective ionic strength (I) given by

$$I = 1/2 \sum m_i z_i^2 \quad (2)$$

where A and B are the Debye-Hückel parameters (Helgeson and Kirkham, 1974; Helgeson et al., 1981) implemented in GEMS using the TSolMod library (Wagner et al., 2012); b_γ is the extended term parameter, which is an empirical parameter that depends on the background electrolyte and was determined previously to have a value of 0.21 for perchloric acid based solutions at temperatures up to 250 °C (Migdisov and Williams-Jones, 2007); $\mathring{a}_i$ is the ion size parameter set

to a value of 4.5 Å for ClO_4^- (Migdisov and William-Jones, 2007) and values for other ions are taken from Kielland (1937); m_i is the molal concentration; z_i is the the charge of the ith aqueous species. The γ_i of neutral species was set to unity, and that of water was calculated from the osmotic coefficient (Helgeson et al., 1981).

The pH is calculated at the experimental temperature using the measured La concentrations in the quenched experimental solutions and the known ClO_4^- concentrations of the experimental starting solutions listed in Table 4. The pH of the experimental aqueous solutions depends on the solubility of La hydroxide and the hydrolysis of La expressed here as formation constants:

$$La(OH)_{3(s)} = La^{3+} + 3OH^- \quad (K_{s0}) \tag{3}$$

$$La^{3+} + OH^- = LaOH^{2+} \quad (\beta_1) \tag{4}$$

$$La^{3+} + 2OH^- = La(OH)_2^+ \quad (\beta_2) \tag{5}$$

$$La^{3+} + 3OH^- = La(OH)_3^0 \quad (\beta_3) \tag{6}$$

where K_{s0} is the solubility product and β_1-β_3 are the equilibrium constants for the formation of La hydroxyl complexes. The $REE(OH)_4^-$ species was omitted in the speciation calculation because this species has not been identified at near-neutral to alkaline pH conditions as determined in the study by Wood et al. (2002) between 50 and 290 °C.

The predicted equilibrium pH is initially calculated using GEMS and the thermodynamic properties of La aqueous species from Supcrt92 (Table 2) to compare the predicted with the experimental La hydroxide solubility data. The final equilibrium pH of the experimental solutions is subsequently re-calculated at temperature during thermodynamic optimization of the La aqueous species using GEMSFITS (Fig. S2).

3.2. Thermodynamic parameter optimization

The program GEMSFITS (Miron et al., 2015) is used for thermodynamic parameter optimization and is coupled with the GEMS3K chemical speciation solver based on Gibbs energy minimization and the TSolMod library (Wagner et al., 2012) also implemented in GEMS (Kulik et al., 2013). GEMSFITS permits conducting simultaneous calculations of equilibrium solubility, speciation, and pH on a large number of experimental data and provides a robust method previously described by Miron et al. (2015). Similar optimizations were applied successfully in previous studies to optimize the hydrolysis constants of Al species and other major cations (Miron et al., 2016, 2017), and to optimize the properties of REE aqueous species (Gysi et al., 2018; Gysi and Harlov, 2021; Pan et al., 2024). Thermodynamic data, equations of state, and activity models used for equilibrium calculations are the same as described above for the GEMS code package.

The thermodynamic optimization procedure involves adjusting the standard partial molal Gibbs energy of formation at temperature T ($\Delta_f G°_T$) of selected La species until GEMSFITS converges. A flowchart showing the calculation sequence is shown in Figure S2. Convergence is achieved when the residuals between the input total dissolved La concentrations measured in the experiments and the calculated output La concentrations are minimized. The equilibrium speciation calculations consider the input La and ClO_4^- concentration of each experiment and equilibrium with La hydroxide solid. The program uses the $\Delta_f G°_T$ values from Tables 2 and 3 for initial speciation calculations at a given temperature, and adjusts the $\Delta_f G°_T$ values for selected La aqueous species and/or La hydroxide solid. This procedure allows minimizing the residuals

between input/output La concentrations (controlled by Eqs. 3-6), re-calculation of pH and full speciation, while maintaining internal thermodynamic consistency between optimized and un-optimized thermodynamic data used in the speciation calculations.

The program uses the bound optimization by quadratic approximation (Powell, 2009), with the sum of residuals as the target parameter that is trying to minimize in each loop until convergence is reached. Other key statistic features for the optimization results include the composite scaled sensitivities (CSS) and the correlation of parameters. The CSS indicates the sensitivity of a parameter to the experimental observations, whereas correlation coefficients calculated for pairs of parameters indicate whether these parameters are correlated to each other (Miron et al., 2015; Tiedeman and Hill, 2007). To allow a better convergence for the optimization of La^{3+} aqua ion, we included experimental data from the ThermoExp_REE database (Pan et al., 2024) for the solubility of monazite ($LaPO_4$) conducted at pH of 2 and at temperatures between 100 to 250 °C.

The aqueous La species considered in the optimizations include the species expected to be stable in acidic to mildly acidic pH. Speciation calculations conducted before any optimizations (Table S1) indicate that La^{3+}, $LaOH^{2+}$ and $La(OH)_2^+$ are the predominant species in the studied pH range and temperature. The $La(OH)_3^0$ species was reaction constrained according to the reaction: $La(OH)_2^+ + OH^- = La(OH)_3^0$ because of its low calculated activities (Table S1).

4. EXPERIMENTAL RESULTS

4.1. Kinetic experiments

A series of kinetic experiments was performed to determine the time required to reach steady-

state dissolved La concentrations in the aqueous solutions equilibrated with La hydroxide. These conditions are interpreted to represent approach to equilibrium conditions. The compositions of the quenched experimental solutions are listed in Table 4.

Figure 3 shows the results of the kinetic runs at 150 and 250 °C with varying starting pH values of 2, 2.5, and 3. All the experiments indicate approach to steady-state La concentrations within 10 to 14 days of reaction depending on the temperature of the experiments regardless of the initial experimental pH. At 150 °C, equilibrium is approached after 11−14 days of reaction, whereas at 250 °C, equilibrium is already approached after 10−12 days of reaction. Replicate experiments conducted for the same isotherm and varying starting pH result in an excellent reproducibility of the experimental data quenched after 11 days of reaction (Table 4). These experiments are therefore selected in this study to further retrieve and evaluate the thermodynamic constants for aqueous La species.

4.2. La hydroxide solubility as a function of temperature and starting pH

The measured compositions of the quenched experimental solutions (equilibrium runs in Table 4) are used to determine the combined effects of temperature and starting pH on the solubility of La hydroxide. The solubility data are initially presented in Figure 4 as the logarithm molality of total dissolved La concentrations (log(mLa)) as a function of starting pH measured at room temperature ($pH_{25°C,initial}$) because the calculated equilibrium pH strongly depends on the hydrolysis of La (Eqs. 4 to 6).

The measured La solubility data display a strong dependence on the starting pH of the experimental solutions (Fig. 4). At initial pH values from 2 to 5, the measured La concentrations

306 decrease from log(*m*La) values of -2.5 to -5.4 at 150 °C, from -2.5 to -5.8 at 200 °C, and from -
307 2.5 to -7.2 at 250 °C. The solubility data in the experiments conducted at 150 and 200 °C are
308 comparable, whereas the La hydroxide solubility decreases more markedly with increased pH at
309 250 °C. Further comparison of the experimental data with the predicted La hydroxide solubility
310 shows an increased divergence for $pH_{25°C,initial}$ values above 3.5 to 5. These differences become
311 more pronounced at elevated temperature, with discrepancies between predictions and
312 experimental data reaching up to 3 orders of magnitude at 250 °C (Fig. 4c). These discrepancies
313 are caused by inaccurate thermodynamic data for the La hydroxyl complexes, which start to
314 prevail with increased pH and temperature (Table S1).

315 To further inspect these discrepancies, a series of speciation calculations was conducted
316 using GEMS, the experimental solution compositions listed in Table 4, and the thermodynamic
317 properties for La species from Sucprt92 (Table 2). The resulting pH values calculated at the
318 experimental temperatures are uncorrected (Table S1, $pH_{T,uncorr}$) and are calculated *a priori* before
319 any optimizations of the thermodynamic properties of La species. The element concentration
320 versus pH solubility profile is generally expected to display a “U-shaped” curve with a decrease
321 in slope with increased pH from acidic to mildly acid, followed by an increase in slope at more
322 alkaline conditions, based on the stepwise hydrolysis of ions (Baes and Mesmer, 1976, 1981).
323 This behavior is related to the stepwise reaction stoichiometry associated to the hydrolysis of La
324 (Eqs. 4-6). Test calculations indicate that the trends observed in a log(*m*La) versus $pH_{T,uncorr}$
325 diagram (Fig. S3) results in erroneous slopes for these solubility profiles, which become
326 pronounced at 250 °C. These significant discrepancies indicate inaccurate pH calculations and a
327 need to re-evaluate the thermodynamic properties of the La aqueous species that control La

hydrolysis in the studied pH range.

5. THERMODYNAMIC OPTIMIZATIONS

5.1. Optimization of La aqueous species

Different optimization modes were tested that involve the adjustment of $\Delta_f G°_T$ values of only one aqueous species (La^{3+}) or simultaneous optimization of two (La^{3+}, $LaOH^{2+}$) or three species (La^{3+}, $LaOH^{2+}$, $La(OH)_2^+$) as well as optimization of the La hydroxide solid. The thermodynamic properties of aqueous La species that do not improve significantly the fits for a given temperature are constrained by assuming their hydrolysis constants to be equal to those derived in the study by Haas et al. (1995). This method maintains internal consistency between the optimized La species and those species that are not optimized.

The results of the optimizations calculations are listed in Table 5. From 150 to 250 °C, simultaneous optimization of $\Delta_f G°_T$ values for the La^{3+}, $LaOH^{2+}$, $La(OH)_2^+$ aqueous species and the La hydroxide solid retrieved the best fit to the experimental La hydroxide solubility data. Figure 5 shows the measured solubility data as a function of the optimized pH values ($pH_{T,opt}$). The optimized solubility profiles are improved because the discrepancies between calculated and measured La concentrations are resolved with residuals generally better than 2.5%. The slopes of the curves in a log(mLa) versus $pH_{T,opt}$ diagram (Fig. 5) are consistent with the stoichiometry of the La hydroxide dissolution and the La hydrolysis reactions (Eqs. 3-5; K_{s0}, β_1 and β_2), which are described by the following three equations:

$$\log a\,(La^{3+}) = \log K_{s0} - 3\log a(OH^-) \quad (7)$$

$$\log a(LaOH^{2+}) = (\log\beta_1 + \log K_{s0}) - 2\log a(OH^-) \quad (8)$$

$$\log a(La(OH)_2^+) = (\log\beta_2 + \log K_{s0}) - \log a(OH^-) \quad (9)$$

where a is the activity of each species. Equation 7 indicates a slope of -3 for the La^{3+} aqua ion, Eq. 8 a slope of -2 for the $LaOH^{2+}$ species, and Eq. 9 a slope of -1 for the $La(OH)_2^+$ species.

The experimental data can be subdivided into two major linear trends with different slopes (Fig. 5) controlled by La^{3+} and $LaOH^{2+}$. The effect of stepwise hydrolysis is reflected by a change in curve slope with increased pH. For example at 150 °C, the fitted slopes are -3.3 at $pH_{T,opt}$ values ranging from 5 to 5.3 and a slope of -2.4 at $pH_{T,opt}$ values ranging from 5.3 to 6. At 200 °C, the fitted curves have slopes of -3.3 at $pH_{T,opt}$ values from 4.1 to 4.5 and -2.1 at $pH_{T,opt}$ values ranging from 4.5 to 5.2. At 250 °C, the data follow linear trends with slope values of -3.3 at $pH_{T,opt}$ from 3.4 to 4 and -2.4 at $pH_{T,opt}$ from 4 to 5. These trends indicate that the two aqueous species La^{3+} and $LaOH^{2+}$ mainly control the solubility of La hydroxides in these experiments, and hence have a higher certainty in these optimization calculations. Note the slight deviations between the slope values derived in Figure 5 and the theoretical slopes presented above. This apparent discrepancy results because the data shown in Figure 5 correspond to the logarithm of total dissolved molality of La and not the calculated activities for La species involved in Eqs. 7-9 (see also Fig. S4).

5.2. Optimized standard partial molal Gibbs energy of formation as a function of temperature

Figure 6 shows the optimized $\Delta_f G°_T$ values for the La aqueous species as a function of temperature with the regressed parameters listed in Table 6. The optimized $\Delta_f G°_T$ values display a close to linear trend with temperature and show significant differences in comparison to the

values predicted from Supcrt92. This is especially pronounced above 150 °C, with differences between ~10 and 12 kJ/mol depending on the La species optimized. From 150 to 250 °C, the optimized $\Delta_f G°_T$ values for La^{3+} are ~1 to 6 kJ/mol more negative than the values predicted from Supcrt92. In contrast, the optimized $\Delta_f G°_T$ values for $LaOH^{2+}$ are ~6 to 11 kJ/mol more positive than the predictions, whereas the adjusted $\Delta_f G°_T$ values for $La(OH)_2^+$ are ~10 to 12 kJ/mol more positive than the predictions. These discrepancies in $\Delta_f G°_T$ values for $La(OH)_2^+$ in turn affect the properties of the $La(OH)_3^0$ species which was reaction constrained (Table 5).

The optimized $\Delta_f G°_T$ values for La hydroxide at 150 °C are -2.9 kJ/mol more negative than predicted based on the data by Diakonov et al. (1998) in Table 3. These differences become significant at high temperature with differences of -11 kJ/mol at 200 °C and -19 kJ/mol at 250 °C (Table 5). Note that the heat capacity derived by Diakonov et al. (1998) displays some uncertainty above 350 K. This is caused by the heat capacity function derived in their study, which is based on calorimetric data by Chirico and Westrum (1980) measured only in the temperature range of 10 to 350 K, whereas at higher temperature a "3*Rn*" equation is derived based on measurements above 200 K. Therefore, a new temperature dependent heat capacity of reaction ($\Delta_r C_P°$) function is derived here (Table 3) by integration of the fitted La hydroxide solubility product vs temperature function, which is derived in Section 6.2.

6. DISCUSSION

6.1. Implications of the optimizations for La speciation as a function of pH

Aqueous speciation was calculated at the experimental conditions using the measured compositions of the quenched experimental solutions (Table 4) and the optimized $\Delta_f G°_T$

parameters for La aqueous species aqueous retrieved in this study (Table 5). Figure 7 shows a comparison between these speciation calculations and the predictions from Supcrt92 between 150 and 250 °C.

The optimized speciation calculations indicate an overall increase in the predominance of the La hydroxyl complexes over the La^{3+} ion with an increase in pH and temperature (Fig. 7a-c). At 150 °C, the La^{3+} aqua ion controls solubility at pH below ~5.3, whereas $LaOH^{2+}$ predominates at pH >5.3 to 6 (Fig. 7a). At 200 °C, there is a shift in predominance of the $LaOH^{2+}$ over the La^{3+} species occurring at pH above ~4.5 (Figure 7b). At 250 °C, the La^{3+} aqua is the predominant species at pH below ~4.1, whereas $LaOH^{2+}$ controls solubility at pH of ~4.2-4.8, and $La(OH)_2^+$ starts to predominate at higher pH values (Figure 7c).

Overall, the calculated speciation is in line with the curve slopes presented in Figure 5 and the reaction stoichiometry from Eqs. 7 and 8, indicating that the La^{3+} aqua ion and the $LaOH^{2+}$ complex are the major species controlling the solubility of La hydroxide in the experiments. The $La(OH)_2^+$ species is expected to become important at pH values above 5.3-6 and at temperatures of 150 and 200 °C, whereas at 250 °C this species becomes predominant at pH close to 5. The $La(OH)_3^0$ species has a minor contribution in controlling La hydroxide solubility at pH below 5-6 in the studied temperature range (Fig. 7a-c).

The aqueous speciation calculated using the thermodynamic data from Supcrt92 (Fig. 7d-f) displays significant differences in comparison to the optimized calculations. Firstly, the total La solubility is generally higher than measured in the experiments. Secondly, the calculated equilibrium pH values are significantly higher (between ~0.2 and 1 pH unit) than those calculated from the optimized La species. This results in a solubility limit for La hydroxide that

is at pH values above ~4.2 to 5.2 depending on temperature. In contrast, those pH solubility limits are much lower in the optimized speciation calculations with values of ~3.4 to 5.

The optimized pH values derived in our study are comparable to the measured *in situ* pH values from the Nd hydroxide solubility study by Wood et al. (2002) (Fig. 8). The lower pH values (between ~0.1 and 0.5 pH units) calculated for some of the experimental data are due to the higher amount of acid used for the pH buffers in our experiments. These results give confidence in the optimized thermodynamic properties for La aqueous species derived in our study, whereas the properties from Supcrt92 result in systematically higher calculated pH values in comparison to other experimental studies (Fig. 8).

6.2. Derivation of the solubility product of La hydroxide and formation constants of La hydroxyl complexes and comparison to literature values

The optimized standard Gibbs energy of formation of the La aqueous species and La hydroxide (Table 5) were used to retrieve the standard Gibbs energy of reaction ($\Delta_r G°$) for Eqs. 3-6 and the equilibrium constants from the relation $\log K = -\Delta_r G°/(RT\ln 10)$, where R is the ideal gas constant and T is temperature in Kelvin. The regressed parameters A_0 to A_4 for the $\log K$ equations as a function of temperature from 25 to 250 °C are listed in Table 7. A comparison between the optimized equilibrium constants and literature values is shown in Figures 9 and 10.

The retrieved solubility products from our study are compared to those by Deberdt et al. (1998) in Figure 9. The latter is to our knowledge the only study that measured the solubility of La hydroxide at elevated temperature. Deberdt et al. (1998) reports solubility data for experiments conducted in NH_4OH/NH_4Cl^- or NaOH/NaCl-based aqueous solutions at 40 to 150

°C and pH from 5 to 9.5. The logK_{s0} value derived by Deberdt et al. (1998) at 150 °C is ~1.5 orders of magnitude higher than our experimental data. In their speciation calculations, Deberdt et al. (1998) assumes that La^{3+} is the only predominant species despite the high pH values reported in those experiments. However, the La aqueous species predicted to control solubility at pH >5.5 to more alkaline pH include $LaOH^{2+}$, $La(OH)_2^{+}$ and $La(OH)_3^{0}$ (Fig. 7). Considering these species, would result in lower calculated La^{3+} activity and hence shift their calculated logK_{s0} values closer to our experimental data.

Solubility data for La hydroxide at 25 °C reported in the literature (Table S3) are mainly sourced from the compilation by Baes and Mesmer (1976) and the critical review by Diakonov et al. (1998). Reported solubility products for REE hydroxides display some variations due to crystallinity and aging of the solids used in the experiments (Diakonov et al., 1998). Values for logK_{s0} of -21.8 and -22.3 are reported by Diakonov et al. (1998) for La hydroxide (aged and crystalline solids). The first value is calculated from mineral thermochemical data, whereas the second one is the calculated average from previously reported solubility data values of -21.7 (Akselrud and Spivakovskii, 1960; Akselrud, 1963; Baes and Mesmer, 1976), -22.8 (Moisa and Spivakovskii, 1970), and -22.4 (Deberdt et al., 1998). The logK_{s0} value of -22.2 used to fit our experimental data at 25 °C (Table 7) is calculated using the $\Delta_f G°_{Tr,\,Pr}$ value for La hydroxide from Diakonov et al. (1998) (Table 3), OH^- from Supcrt92 (Table 2) and the fitted parameters for La^{3+} derived in this study (Table 6). The latter logK_{s0} value falls between the range of literature solubility data at reference temperature (Fig. 9).

Experimental data for the hydrolysis of La and other REE at 25 °C are commonly sourced from the extensive reviews by Baes and Mesmer (1976, 1981) and Lee and Byrne (1992). In the

former studies, the reported average logβ_1 value for La hydrolysis is 5.5, whereas in the study of Lee and Byrne (1992) the calculated logβ_1, logβ_2, and logβ_3 values are 5.3, 9.9 and 14.1, respectively (Table S4). The La hydrolysis constants reported by Haas et al. (1995) and used in Supcrt92 are based on the 25 °C data by Lee and Byrne (1992), which were also used to constrain the fits to our experimental data in Figure 10. Klungness and Byrne (2000) conducted potentiometric experiments between 25 and 55 °C and reported a function for the temperature dependence of the first hydrolysis constant of La, with calculated logβ_1 values of 5.2 at 25 °C and 5.1 at 55 °C, respectively. These values are 0.2 to 0.8 log units lower than our experimental fits and those predicted using Supcrt92 and do not show an expected increase with temperature. Stepanchikova et al. (2014) measured the stepwise stability constants for La hydroxyl complexes at 25 °C, with retrieved β_1-β_3 values up to 3 log units higher than those derived from previous work and this study (Table S4). Figure 10 shows that the predicted β_1-β_3 at elevated temperatures based on data from Supcrt92 closely approach the fits to our experimental data at temperatures below 75 °C. In contrast, the predicted formation constants are higher than experiments at temperatures above 75 °C. This divergence becomes increasingly significant with temperature and reaches up to ~2 orders of magnitude at 250 °C.

6.3. Comparison to other hydrothermal REE speciation studies

The study by Wood et al. (2002) is to our knowledge the only other experimental study that reports the formation constants for the hydrolysis of REE at temperatures above 100 °C. Their study reports the Nd hydrolysis formation constants β_1 at 250 and 290 °C and β_2-β_3 at 290 °C. A comparison of these Nd hydrolysis constants for $NdOH^{2+}$, $Nd(OH)_2^{+}$ and $Nd(OH)_3^{0}$ with those

calculated from the HKF parameters derived by Haas et al. (1995) indicates an overestimation of the stability of $NdOH^{2+}$ and $Nd(OH)_2^{+}$ over the Nd^{3+} species at 290 °C and acidic pH (Migdisov et al., 2016). Furthermore, these experiments indicate a predominance of the Nd^{3+} ion over the $NdOH^{2+}$ species at pH between 2 to ~3.2, whereas $NdOH^{2+}$ predominates at pH of ~3.2-5 (Fig. S5). These observations are in line with the speciation of La optimized in our study (Fig. 7c), which shows a predominance of La^{3+} over $LaOH^{2+}$ at pH values >2 to ~4 at 250 °C. Moreover, the discrepancies between the experimental values for β_1-β_3 for Nd hydrolysis from Wood et al. (2002) and those predicted (Haas et al., 1995) at 250 to 290 °C range between 1.8 to 3.4 orders of magnitude. These discrepancies are comparable to those determined in our study at 250 °C and further extrapolation to 290 °C (Fig. 10, Table 8).

Other studies that report the stability of the REE^{3+} aqua ions and the $REEOH^{2+}$ species at hydrothermal conditions are based on REE phosphate solubility experiments (Gysi et al., 2015, 2018; Van Hoozen et al., 2020; Gysi and Harlov, 2021). Van Hoozen et al. (2020) conducted synthetic $LaPO_4$ monazite solubility experiments from 100 to 250 °C in perchloric acid-based buffer solutions with pH of 2. These experimental data are internally consistent with our study because they were used in the optimization of the La^{3+} aqua ion listed in Table 5. Pan et al. (2024) performed similar optimization calculations of a large compilation of hydrothermal monazite solubility experiments, including the data by Van Hoozen et al. (2020). However, a major difference with our study is that the standard partial molal Gibbs energies of the La^{3+} aqua ions and the $LaOH^{2+}$ species were only optimized at at reference temperature and pressure to keep internal consistency with the HKF parameters listed in Haas et al. (1995). However, in the present study, we demonstrate the need for optimizing the temperature functions for the La

aqueous species (Fig. 6), which is now possible because our solubility experiments were conducted as a function of both pH and temperature.

6.4. Implications on predicted monazite solubility and aqueous speciation in hydrothermal fluids

The solubility of monazite ($LaPO_4$) was modeled in NaCl-bearing fluids as a function of pH and salinity at 250 °C to evaluate the controls of chloride vs hydroxyl complexes on the mobility of La in hydrothermal fluids (Fig. 11). Overall, the solubility of monazite strongly depends on pH and indicates that the mobility of La in acidic and alkaline fluids is significantly higher than that in mildly acidic to near neutral fluids. Moreover, this mobility increases with increased salinity.

The calculated aqueous speciation indicates that the La^{3+} ion and the chloride complexes ($LaCl^{2+}$ and $LaCl_2^{+}$) have a predominant role in controlling $LaPO_4$ solubility over the La hydroxyl complexes at acidic to mildly acidic pH, whereas the La hydroxyl complexes predominate at higher pH. Increasing salinity to 0.1 M NaCl results in an overall increased total dissolved log(*m*La) by ~0.3 to 0.6 units and expands the predominance field of the La chloride complexes to a pH up to ~5.5 (Fig. 11b). These calculations support results from previous experimental and modeling studies that have demonstrated the importance of chloride-bearing species for REE transport in NaCl-bearing fluids (Migdisov et al., 2009, 2016; Gysi and Williams-Jones, 2013; Migdisov and Williams-Jones, 2014; Perry and Gysi, 2018).

The La hydroxyl complexes control the solubility of $LaPO_4$ at pH higher than ~4.5-5.5, depending on salinity of the model (Fig. 11). The $La(OH)_3^0$ species predominates with increased pH but the accuracy of these calculations is currently unknown and warrants future experiments

for determining the stability of this species in alkaline solutions.

7. CONCLUSIONS

The solubility of La hydroxide was determined between 150 and 250 °C and at acidic to mildly acidic pH. Thermodynamic optimizations of these new solubility data and existing literature data permit deriving the equilibrium constants (K_{s0} and β_1-β_3) for the stability of La^{3+}, $LaOH^{2+}$, $La(OH)_2^+$, and $La(OH)_3^0$ aqueous species between 25 and 250 °C (Table 7). The three major La species controlling solubility in the experimental pH and temperature range studied include La^{3+}, $LaOH^{2+}$, and $La(OH)_2^+$. Updates of the thermodynamic properties for La aqueous species results in a higher stability of the La^{3+} aqua ion over the La hydroxyl complexes in comparison to previous predictions using thermodynamic data reported by Haas et al. (1995) or Supcrt92. The La^{3+} aqua ion is predominant up to pH of ~5.3 at 150 °C, pH of 4.5 at 200 °C, and pH of 4 at 250 °C, whereas at higher pH, the speciation becomes controlled by $LaOH^{2+}$. The experimentally derived formation constants for the La hydroxyl species from 150 to 250 °C further indicate that the La hydroxyl complexes become stable towards more acidic pH values with increased temperature, and therefore, these species are expected to start playing an important role for REE mobilization in high temperature and more alkaline fluids.

CREDIT AUTHOR STATEMENT

Kevin Padilla: Conceptualization, Methodology, Formal analysis, Investigation, Data curation, Writing – original draft, Writing – review & editing. **Alexander P. Gysi:** Conceptualization,

Methodology, Formal analysis, Data curation, Writing – review & editing, Supervision, Project administration, Funding acquisition.

ACKNOWLEDGMENTS

This research is based upon work supported by the U.S. Department of Energy, Office of Science, Office of Basic Energy Sciences, Geosciences program under Award Number DE-SC0021106 (experimental work) and DE-SC0022269 (thermodynamic optimizations and databases) to APG. We are grateful for the useful comments by N. Hurtig and J. Rakovan on solids characterization. We would like to thank H. Han and B. Frey for assistance on ICP-OES and ICP-MS analysis at the New Mexico Bureau of Geology and Mineral Resources. D. Kulik and G. D. Miron are thanked for providing guidance on GEMSFITS calculations. This manuscript benefited considerably from the constructive comments by two anonymous reviewers. We thank Guest Associate Editor Kono Lemke and Executive Editor Jeffrey Catalano for their useful comments and for handling this manuscript.

APPENDIX A. SUPPLEMENTARY MATERIAL

Supplementary materials include comparison of measured and modeled XRD spectra with reference patterns (Fig. S1), flowchart for the thermodynamic optimization process (Fig. S2), solubility profiles showing the measured La concentrations vs calculated pH before optimizations (Fig. S3), comparison of log molality and log activity vs pH solubility profiles (Fig. S4), comparison of La speciation model with previous experimental study on Nd speciation (Fig. S5). Also included, the calculated speciation of experimental solutions using La species from Sucprt92 (Table S1) and the optimized La species in this study (Table S2). Optimized K_{s0}

and β_1-β_3 values from this study calculated at different temperatures are compared to literature values in Tables S3 to S4. The simulated speciation data for the solubility of monazite is listed in Table S5.

DATA AVAILABILITY

Data are available through Mendeley Data at https://doi.org/10.17632/smjc94j5sw.1

REFERENCES

Aries S., Valladon M., Polvé M. and Dupré B. (2000) A routine method for oxide and hydroxide interference corrections in ICP-MS chemical analysis of environmental and geological samples. Geostand. Newslett. 24, 19-31.

Akselrud N. V. and Spivakovskii V. B. (1960) Hydroxides and basic chlorides of yttrium and lantanum. Russ. J. Inorg. Chem. 5, 158–163.

Akselrud N. V. (1963) Hydroxychlorides and hydroxides of the elements scandium and lanthanides. Uspehi Khimii 32, 800822, in Russian.

Baes Jr. C. F. and Mesmer R. E. (1976) The Hydrolysis of Cations. Wiley, New York, 489 pp.

Baes Jr. C. F. and Mesmer R. E. (1981) The thermodynamics of cation hydrolysis. Am. J. Sci. 281, 935-962.

Beall G. W., Milligan W. O. and Wolcott H. A. (1977) Structural trends in the lanthanide trihydroxides. J. Inor. Nucl. Chem. 39, 65–70.

Beland C. M. and Williams-Jones A. E. (2021) The genesis of the Ashram REE deposit, Quebec: Insights from bulk-rock geochemistry, apatite-monazite-bastnäsite replacement reactions and

592 mineral chemistry. Chem. Geol. 578, 120298.
593 Chirico R. D. and Westrum Jr E. F. (1980) Thermophysics of the lanthanide hydroxides I. Heat
594 capacities of La $(OH)_3$, Gd $(OH)_3$, and $Eu(OH)_3$ from near 5 to 350 K. Lattice and Schottky
595 contributions. J. Chem. Thermodyn. 12, 71–85.
596 Choppin G. R., Kelly D. A. and Ward E. E. (1966) Effect of changes in the ionic medium on the
597 stability constant of $Eu(NO_3)^{2+}$, AEC Access. Nos. (ORO-1797-2), 21pp.
598 Cook N. J., Ciobanu C. L., O'Rielly D., Wilson R., Das K. and Wade B. (2013) Mineral
599 chemistry of Rare Earth Element (REE) mineralization, Browns Ranges, Western Australia.
600 Lithos 172–173, 192–213.
601 Cordfunke E. H. P., Konings R. J. M. and Ouweltjes W. (1990) The standard enthalpies of
602 formation of hydroxides IV. $La(OH)_3$ and LaOOH. J. Chem. Thermodyn. 22, 449–452.
603 Deberdt S., Castet S., Dandurand J. L., Harrichoury J. C. and Louiset I. (1998) Experimental
604 study of $La(OH)_3$ and $Gd(OH)_3$ solubilities (25 to 150 °C), and La–acetate complexing (25 to
605 80 °C). Chem. Geol. 151, 349–372.
606 Diakonov I. I., Ragnarsdottir K. V. and Tagirov B. R. (1998) Standard thermodynamic properties
607 and heat capacity equations of rare earth hydroxides: II. Ce(III)-, Pr-, Sm-, Eu(III)-, Gd-, Tb-,
608 Dy-, Ho-, Er-, Tm-, Yb-, and Y-hydroxides. Comparison of thermochemical and solubility
609 data. Chem. Geol. 151, 327–347.
610 Dordevic V., Antic Z., Nikolic M. G. and Dramicanin M. D. (2014) Comparative structural and
611 photoluminescent study of Eu^{3+}-doped La_2O_3 and $La(OH)_3$ nanocrystalline powders. Journal
612 of Physics and Chemistry of Solids 75, 276–282.
613 Goodenough K. M., Wall F. and Merriman D. (2018) The rare earth elements: demand, global

resources, and challenges for resourcing future generations. Nat. Resour. Res. 27, 201–216.

Gysi A. P. and Williams-Jones A. E. (2013) Hydrothermal mobilization of pegmatite-hosted REE and Zr at Strange Lake, Canada: A reaction path model. Geochim. Cosmochim. Acta 122, 324–352.

Gysi A. P. and Harlov D. (2021) Hydrothermal solubility of $TbPO_4$, $HoPO_4$, $TmPO_4$, and $LuPO_4$ xenotime endmembers at pH of 2 and temperatures between 100 and 250 °C. Chem. Geol. 567, 120072.

Gysi A. P., Williams-Jones A. E. and Harlov D. (2015) The solubility of xenotime-(Y) and other HREE phosphates ($DyPO_4$, $ErPO_4$ and $YbPO_4$) in aqueous solutions from 100 to 250 °C and psat. Chem. Geol. 401, 83–95.

Gysi A. P., Williams-Jones A. E. and Collins P. (2016) Lithogeochemical vectors for hydrothermal processes in the Strange Lake peralkaline granitic REE-Zr-Nb deposit. Econ. Geol. 111, 1241–1276.

Gysi A. P., Harlov D. and Miron G. D. (2018) The solubility of monazite ($CePO_4$), $SmPO_4$, and $GdPO_4$ in aqueous solutions from 100 to 250 °C. Geochim. Cosmochim. Acta 242, 143–164.

Gysi A. P., Hurtig N. C., Pan R., Miron G. D., and Kulik D. A. (2023) MINES thermodynamic database, New Mexico Bureau of Geology and Mineral Resources, version 23, https://doi.org/10.58799/mines-tdb.

Haas J. R., Shock E. L. and Sassani D. C. (1995) Rare earth elements in hydrothermal systems: Estimates of standard partial molal thermodynamic properties of aqueous complexes of the rare earth elements at high pressures and temperatures. Geochim. Cosmochim. Acta 59, 4329–4350.

Han H. J. and Gysi A. P. (2024) UV-Vis spectrophotometric determination of rare earth elements (REE) speciation at near-neutral to alkaline pH. Part I: m-cresol purple properties from 25–75 °C and Er hydrolysis. *Dalton Trans.*

Harlov D. E., Meighan C. J., Kerr I. D. and Samson I. M. (2016) Mineralogy, chemistry, and fluid-aided evolution of the Pea Ridge Fe oxide-(Y + REE) deposit, southeast Missouri, USA. Econ. Geol. 111, 1963–1984.

Hatch G. P. (2012) Dynamics in the global market for rare earths. Elements 8, 341–346.

Helgeson H. C. and David H. Kirkham (1974) Theoretical prediction of the thermodynamic behavior of aqueous electrolytes at high pressures and temperatures; II, Debye-Hückel parameters for activity coefficients and relative partial molal properties. Am. J. Sci. 274, 1199–1261.

Helgeson H. C., Kirkham D. H. and Flowers G. C. (1981) Theoretical prediction of the thermodynamic behavior of aqueous electrolytes by high pressures and temperatures; IV, Calculation of activity coefficients, osmotic coefficients, and apparent molal and standard and relative partial molal properties to 600 °C and 5kb. Am. J. Sci. 281, 1249–1516.

Johnson J. W., Oelkers E. H. and Helgeson H. C. (1992) SUPCRT92: A software package for calculating the standard molal thermodynamic properties of minerals, gases, aqueous species, and reactions from 1 to 5000 bar and 0 to 1000 °C. Comput. Geosci. 18, 899–947.

Kestin J., Sengers J. V., Kamgar-Parsi B. and Levelt Sengers J. M. H. (1984) Thermophysical properties of fluid H_2O. J. Phys. Chem. Ref. Data 13, 175–183.

Kielland J. (1937) Individual activity coefficients of ions in aqueous solutions. J. Am. Chem. Soc. 59, 1675–1678.

Klungness G. D. and Byrne R. H. (2000) Comparative hydrolysis behavior of the rare earths and yttrium: the influence of temperature and ionic strength. Polyhedron 19, 99–107.

Kulik D. A., Wagner T., Dmytrieva S. V., Kosakowski G., Hingerl F. F., Chudnenko K. V. and Berner U. R. (2013) GEM-Selektor geochemical modeling package: revised algorithm and GEMS3K numerical kernel for coupled simulation codes. Comput. Geosci. 17, 1–24.

Lee J. H. and Byrne R. H. (1992) Examination of comparative rare earth element complexation behavior using linear free-energy relationships. Geochim. Cosmochim. Acta 56, 1127–1137.

Liu S., Ding L., Fan H.-R., Yang K.-F., Tang Y.-W., She H.-D. and Hao M. (2020) Hydrothermal genesis of Nb mineralization in the giant Bayan Obo REE-Nb-Fe deposit (China): implicated by petrography and geochemistry of Nb-bearing minerals. Precambrian Res. 348, 105864.

Louvel M., Etschmann B., Guan Q., Testemale D. and Brugger J. (2022) Carbonate complexation enhances hydrothermal transport of rare earth elements in alkaline fluids. Nat. Commun. 13, 1456.

Lutterotti, L. (2000) Maud: a Rietveld analysis program designed for the internet and experiment integration. Acta Crystallogr. A56,54.

Merli L., Lambert B. and Fuger J. (1997) Thermochemistry of lanthanum, neodymium, samarium and americium trihydroxides and their relation to the corresponding hydroxycarbonates. J. Nucl. Mater. 247, 172–176.

Migdisov A. A. and Williams-Jones A. E. (2007) An experimental study of the solubility and speciation of neodymium (III) fluoride in F-bearing aqueous solutions. Geochim. Cosmochim. Acta 71, 3056–3069.

Migdisov A. A. and Williams-Jones A. E. (2008) A spectrophotometric study of Nd(III), Sm(III)

and Er(III) complexation in sulfate-bearing solutions at elevated temperatures. Geochim. Cosmochim. Acta 71, 72, 5291–5303.

Migdisov A. A. and Williams-Jones A. E. (2014) Hydrothermal transport and deposition of the rare earth elements by fluorine-bearing aqueous liquids. Miner. Depos. 49, 987–997.

Migdisov A. A., Williams-Jones A. E. and Wagner T. (2009) An experimental study of the solubility and speciation of the Rare Earth Elements (III) in fluoride- and chloride-bearing aqueous solutions at temperatures up to 300°C. Geochim. Cosmochim. Acta 73, 7087–7109.

Migdisov A. A., Williams-Jones A. E., Brugger J. and Caporuscio F. A. (2016) Hydrothermal transport, deposition, and fractionation of the REE: Experimental data and thermodynamic calculations. Chem. Geol. 439, 13–42.

Migdisov A. A., Guo X., Nisbet H., Xu H. and Williams-Jones A. E. (2019) Fractionation of REE, U, and Th in natural ore-forming hydrothermal systems: Thermodynamic modeling. J. Chem. Thermodyn. 128, 305–319.

Miron G. D., Kulik D. A., Dmytrieva S. V. and Wagner T. (2015) GEMSFITS: Code package for optimization of geochemical model parameters and inverse modeling. Appl. Geochem. 55, 28–45.

Miron G. D., Wagner T., Kulik D. A. and Heinrich C. A. (2016) Internally consistent thermodynamic data for aqueous species in the system Na–K–Al–Si–O–H–Cl. Geochim. Cosmochim. Acta 187, 41–78.

Miron G. D., Wagner T., Kulik D. A. and Lothenbach B. (2017) An internally consistent thermodynamic dataset for aqueous species in the system Ca-Mg-Na-K-Al-Si-OHC-Cl to 800 °C and 5 kbar. Am. J. Sci. 317, 755–806.

Moisa L. P. and Spivakovskii V. B. (1970) Conditions of precipitation of hydroxichlorides and hydroxides of lantanum from chloride solutions. Zhurnal Neorganicheskoy Khimii 15, 2907–2913, in Russian.

Moore M., Chakhmouradian A. R., Mariano A. N. and Sidhu R. (2015) Evolution of rare-earth mineralization in the Bear Lodge carbonatite, Wyoming: mineralogical and isotopic evidence. Ore Geol. Rev. 64, 499–521.

Navrotsky A., Lee W., Mielewczyk-Gryn A., Ushakov S. V., Anderko A., Wu H. and Riman R. C. (2015) Thermodynamics of solid phases containing rare earth oxides. J. Chem. Thermodyn. 88, 126–141.

Nisbet H., Migdisov A. A., Goncharov V., van Hinsberg V., Williams-Jones A. E., Xu H. and Guo X. (2022) The solubility and speciation of Nd in carbonate-bearing hydrothermal fluids up to 250 °C. Chem. Geol. 611, 121122.

Pan R., Gysi A. P., Miron G. D. and Zhu, C. (2024) Optimized thermodynamic properties of REE aqueous species (REE^{3+} and $REEOH^{2+}$) and experimental database for modeling the solubility of REE phosphate minerals (monazite, xenotime, and rhabdophane) from 25 to 300 °C. Chem. Geol. 643, 121817.

Perry E. P. and Gysi A. P. (2018) Rare earth elements in mineral deposits: speciation in hydrothermal fluids and partitioning in calcite. Geofluids 2018, 1–19.

Powell M. J. (2009) The BOBYQA algorithm for bound constrained optimization without derivatives. Cambridge NA Report NA2009/06, University of Cambridge, Cambridge 26, 26–46.

Roy R. and McKinstry H. A. (1953) Concerning the so-called $Y(OH)_3$-type structure and the

724 structure of $La(OH)_3$. Acta Cryst 6, 365–366.
725 Salvi S. and Williams-Jones A. E. (1996) The role of hydrothermal processes in concentrating
726 high-field strength elements in the Strange Lake peralkaline complex, northeastern Canada.
727 Geochim. Cosmochim. Acta 60, 1917–1932.
728 Salvi S. and Williams-Jones A. E. (2006) Alteration, HFSE mineralisation and hydrocarbon
729 formation in peralkaline igneous systems: Insights from the Strange Lake Pluton, Canada.
730 Lithos 91, 19–34.
731 Shock E. L. and Helgeson H. C. (1988) Calculation of the thermodynamic and transport
732 properties of aqueous species at high pressures and temperatures: Correlation algorithms for
733 ionic species and equation of state predictions to 5 kb and 1000 °C. Geochim. Cosmochim.
734 Acta 52, 2009–2036.
735 Shock E. L., Helgeson H. C. and Sverjensky D. A. (1989) Calculation of the thermodynamic and
736 transport properties of aqueous species at high pressures and temperatures: standard partial
737 molal properties of inorganic neutral species. Geochim. Cosmochim. Acta 53, 2157–2183.
738 Shock E. L., Oelkers E. H., Johnson J. W., Sverjensky D. A. and Helgeson H. C. (1992)
739 Calculation of the thermodynamic properties of aqueous species at high pressures and
740 temperatures. Effective electrostatic radii, dissociation constants and standard partial molal
741 properties to 1000 °C and 5 kbar. J. Chem. Soc., Faraday Trans. 88, 803–826.
742 Shock E. L., Sassani D. C., Willis M. and Sverjensky D. A. (1997) Inorganic species in geologic
743 fluids: Correlations among standard molal thermodynamic properties of aqueous ions and
744 hydroxide complexes. Geochim. Cosmochim. Acta 61, 907–950.
745 Smith M. P., Henderson P. and Campbell L. S. (2000) Fractionation of the REE during

746 hydrothermal processes: constraints from the Bayan Obo Fe-REE-Nb deposit, Inner
747 Mongolia, China. Geochim. Cosmochim. Acta 64, 3141–3160.
748 Smith M. P., Campbell L. S. and Kynicky J. (2015) A review of the genesis of the world class
749 Bayan Obo Fe–REE–Nb deposits, Inner Mongolia, China: multistage processes and
750 outstanding questions. Ore Geol. Rev. 64, 459–476.
751 Stepanchikova S. A., Biteikina R. P., Shironosova G. P. and Kolonin G. R. (2014) An
752 experimental study of hydroxo complex formation in basic and near-neutral solutions of rare-
753 earth elements and yttrium at 25 °C. Russian Geology and Geophysics 55, 941–944.
754 Tanger J. C. and Helgeson H. C. (1988) Calculation of the thermodynamic and transport
755 properties of aqueous species at high pressures and temperatures; revised equations of state
756 for the standard partial molal properties of ions and electrolytes. Am. J. Sci. 288, 19–98.
757 Tiedeman C. R. and Hill M. C. (2007) Model calibration and issues related to validation,
758 sensitivity analysis, post-audit, uncertainty evaluation and assessment of prediction data
759 needs. In Groundwater: Resource Evaluation, Augmentation, Contamination, Restoration,
760 Modeling and Management Springer. pp. 237–282.
761 Van Hoozen C. J., Gysi A. P. and Harlov D. E. (2020) The solubility of monazite ($LaPO_4$, $PrPO_4$,
762 $NdPO_4$, and $EuPO_4$) endmembers in aqueous solutions from 100 to 250 °C. Geochim.
763 Cosmochim. Acta 280, 302–316.
764 Vasyukova O. V. and Williams-Jones A. E. (2019) Closed system fluid-mineral-mediated trace
765 element behaviour in peralkaline rare metal pegmatites: Evidence from Strange Lake. Chem.
766 Geol. 505, 86–99.
767 Wagner T., Kulik D. A., Hingerl F. F. and Dmytrieva S. V. (2012) GEM-Selektor geochemical

modeling package: TSolMod library and data interface for multicomponent phase models. Can. Mineral. 50, 1173–1195.

Williams-Jones A. E., Migdisov A. A. and Samson I. M. (2012) Hydrothermal mobilisation of the rare earth elements-a tale of “ceria” and “yttria.” Elements 8, 355–360.

Williams-Jones A. E., Samson I. M. and Olivo G. R. (2000) The genesis of hydrothermal fluorite-REE deposits in the Gallinas Mountains, New Mexico. Econ. Geol. 95, 327–341.

Wood S. A. (1990) The aqueous geochemistry of the rare-earth elements and yttrium 2. Theoretical predictions of speciation in hydrothermal solutions to 350 °C at saturation water vapor pressure. Chem. Geol. 88, 99–125.

Wood S. A., Palmer D. A., Wesolowski D. J. and Benezeth P. (2002) The aqueous geochemistry of the rare earth elements and yttrium. Part XI. The solubility of $Nd(OH)_3$ and hydrolysis of Nd^{3+} from 30 to 290 °C at saturated water vapor pressure with in-situ pHm measurement. Water-Rock Interact. Ore Depos., Environ. Geochem Tribut. to David A. Crerar Spec. Publ. 7, 229–256.

FIGURES

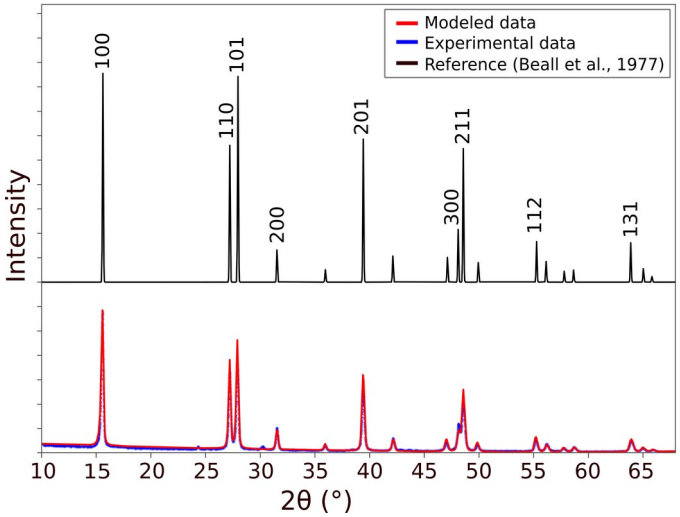

Fig. 1. X-ray diffractograms of La hydroxide powders synthesized hydrothermally at 250 °C and used in this study, showing the measured and modeled (Rietveld refinement) spectra. The spectra match the La hydroxide reference spectrum by Beall et al. (1977) with the hexagonal ($P6_3/m$) crystal structure with numbers indicating Bragg indices for major reflections.

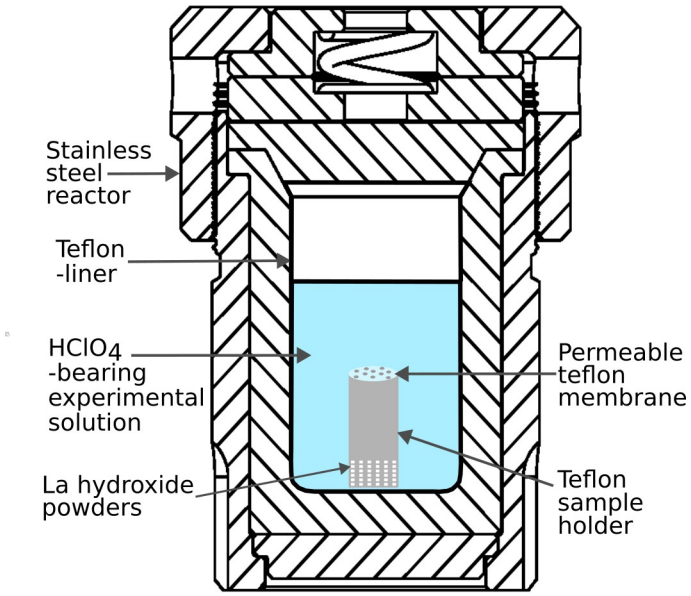

Fig. 2. Schematic of the experimental design showing a batch-type Teflon-lined stainless steel batch-type reactor and sample holder used to measure the solubility of La hydroxide in perchloric acid-based solutions.

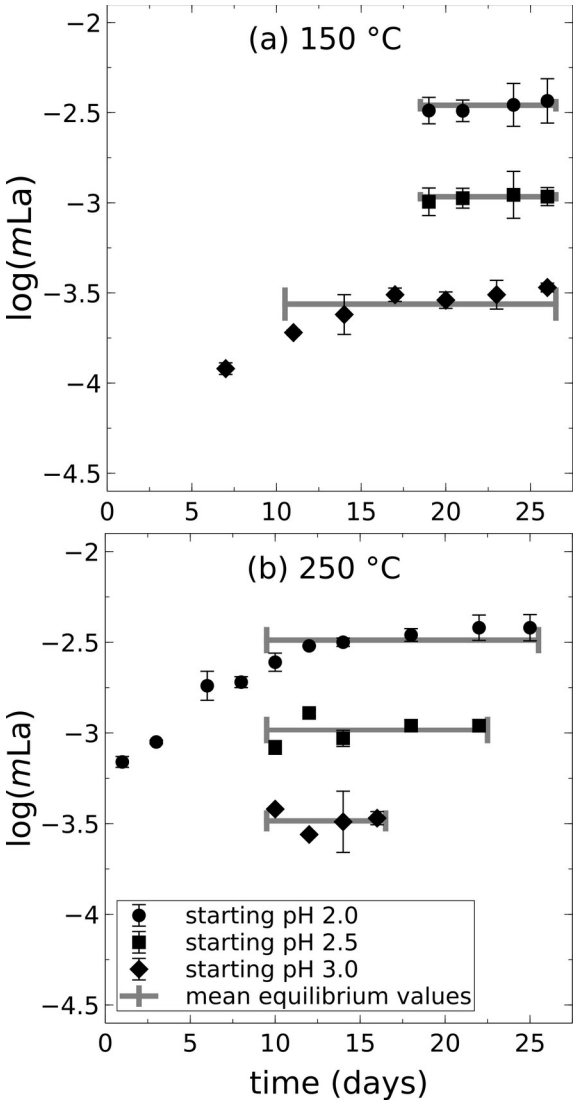

Fig. 3. Logarithm molality of La (mol/kg) measured in the quenched experimental solutions as a function of time (days) showing kinetic plots at (a) 150 °C and (b) 250 °C and different starting pH values of 2 to 3. Grey lines represent the mean values for experimental data conducted over 11 days of reaction and end bars represent their standard deviations (1σ). Experimental data are listed in Table 4.

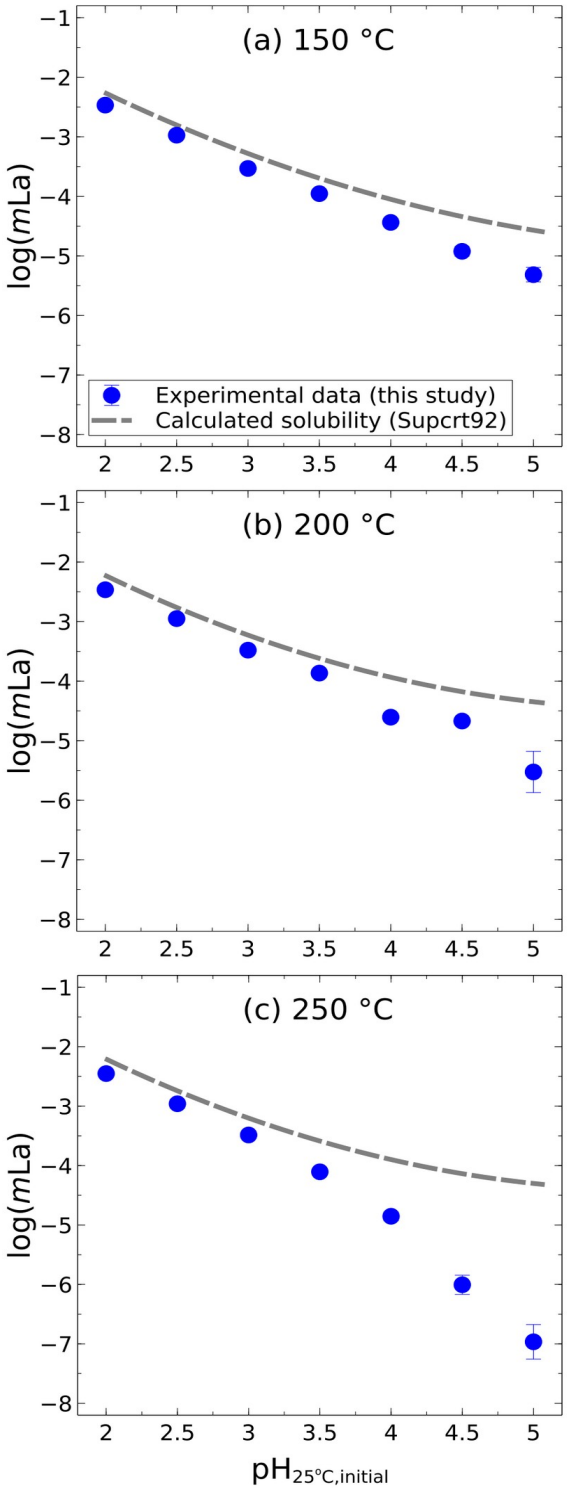

Fig. 4. Logarithm molality of La (mol/kg) measured in the quenched experimental solutions at (a) 150, (b) 200 and (c) 250 °C as a function of starting pH of the experimental buffer solutions at room temperature. The calculated La hydroxide solubility is determined from the thermodynamic properties of the La^{3+} aqua ion and La hydroxyl species compiled in Supcrt92

807 (Table 2) combined with the La hydroxide properties from Table 3. The error bars or symbol
808 sizes represent the standard deviation (1σ) values from replicate experiments with the
809 experimental data listed in Table 4.
810

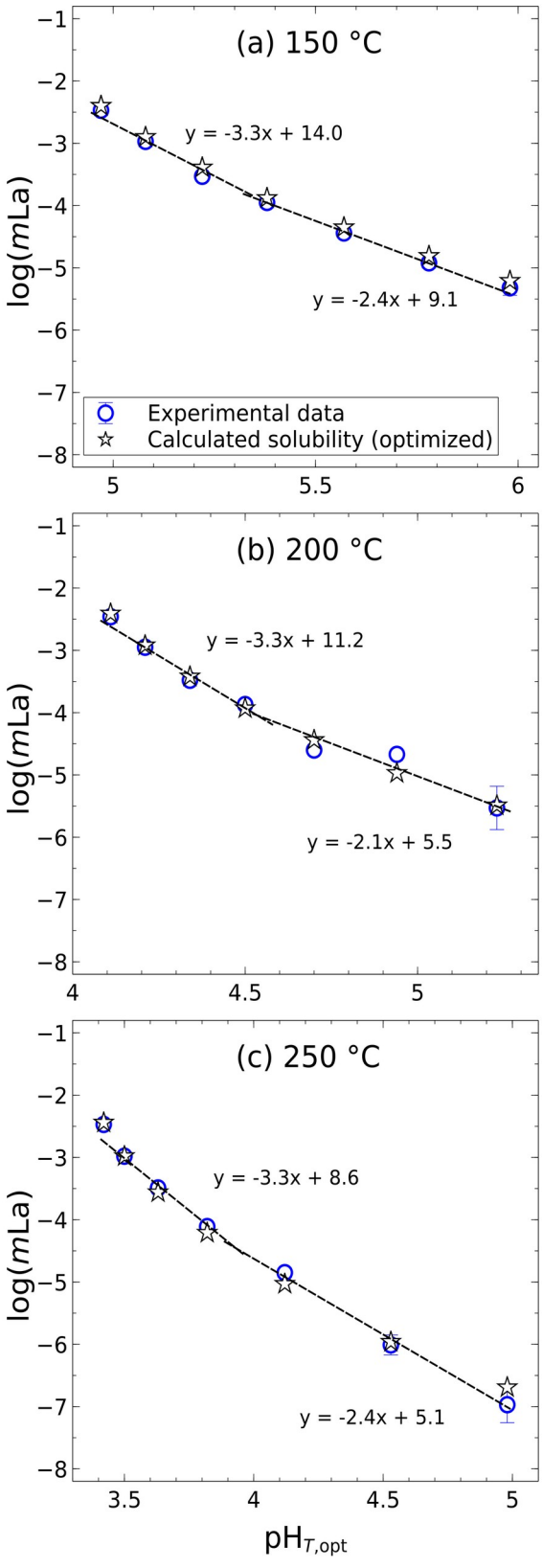
(a) 150 °C
y = -3.3x + 14.0
y = -2.4x + 9.1
Experimental data
Calculated solubility (optimized)
(b) 200 °C
y = -3.3x + 11.2
y = -2.1x + 5.5
(c) 250 °C
y = -3.3x + 8.6
y = -2.4x + 5.1
log(mLa)
pH$_{T,opt}$

811

Fig. 5. Logarithm molality of La (mol/kg) measured in the quenched experimental solutions as a function of pH at (a) 150, (b) 200 and (c) 250 °C at saturated water vapor pressure. The slopes of the curves are related to La^{3+} and to $LaOH^{2+}$ controlling solubility (Eqs. 7-8, slopes of -3 and -2). The calculated optimized pH values ($pH_{T,opt}$) and La solubility are listed in Table S2.

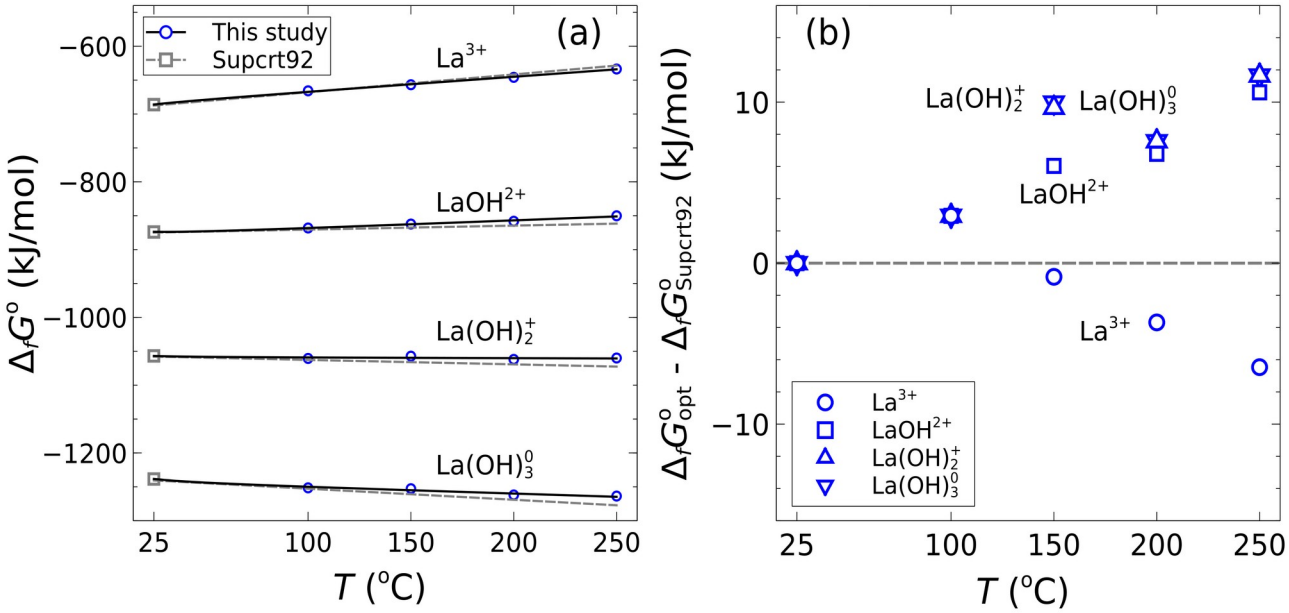

Fig. 6. (a) Optimized standard partial molal Gibbs energy ($\Delta_f G°$) of La aqueous species retrieved from La hydroxide and monazite-(La) solubility experiments as a function of temperature (°C), and comparison to predicted values from Supcrt92. (b) Calculated residuals between experimental and predicted Gibbs energy values ($\Delta_f G°_{opt}$ - $\Delta_f G°_{Supcrt92}$). The regressed parameters for the fits in (a) are listed in Table 6. Data at 25 °C are from Supcrt92 and the optimized values at 100 °C are based on monazite solubility data from Van Hoozen et al. (2020).

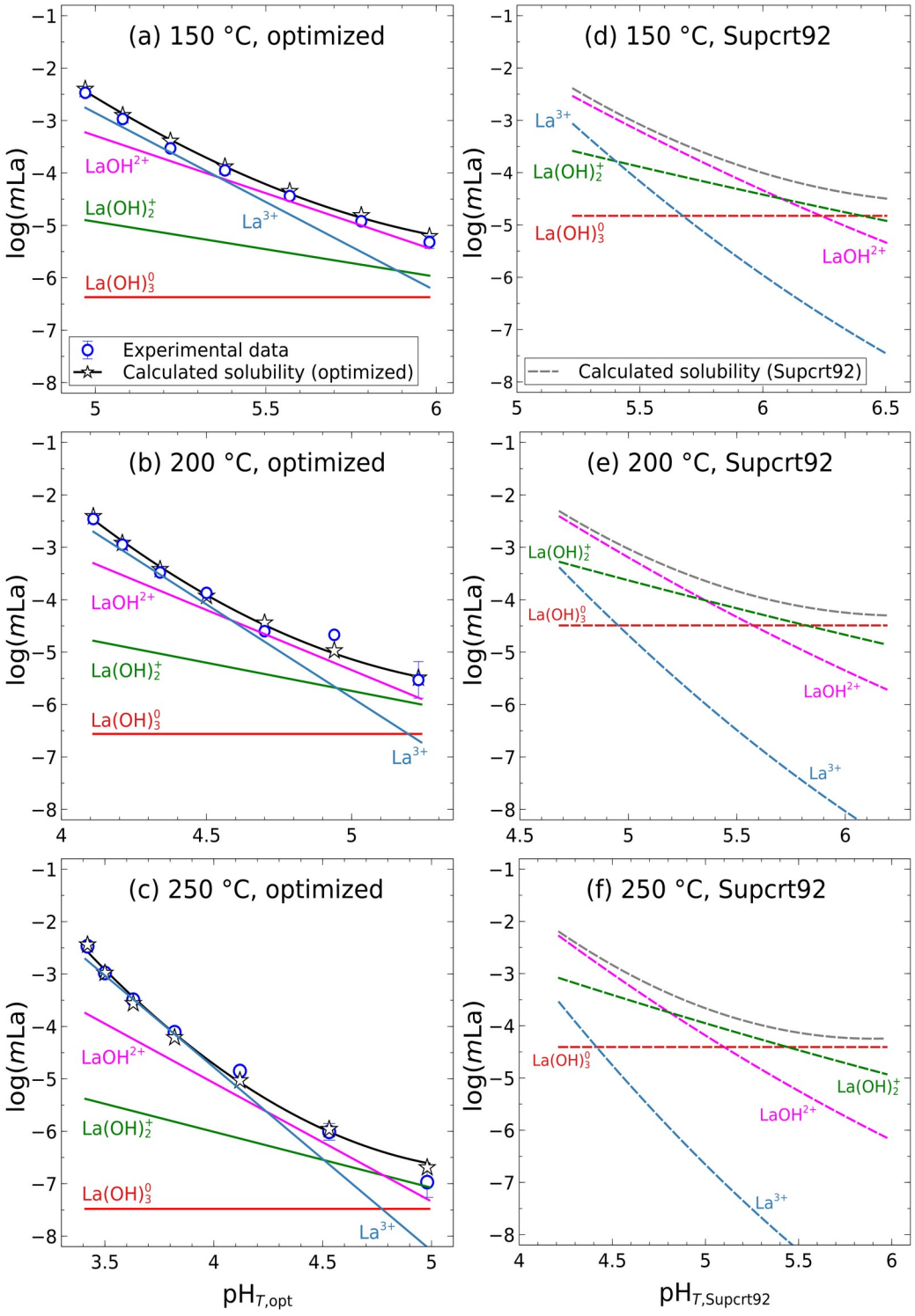
(a) 150 °C, optimized
(b) 200 °C, optimized
(c) 250 °C, optimized
(d) 150 °C, Supcrt92
(e) 200 °C, Supcrt92
(f) 250 °C, Supcrt92
log(mLa)
pH$_{T,opt}$
pH$_{T,Supcrt92}$
LaOH^{2+}
La(OH)$_2^+$
La(OH)$_3^0$
La^{3+}
Experimental data
Calculated solubility (optimized)
Calculated solubility (Supcrt92)

825

Fig. 7. Measured and calculated logarithm molality (in mol/kg) of total dissolved La concentrations and stability of La aqueous species (La^{3+}, $LaOH^{2+}$, $La(OH)_2^{+}$ and $La(OH)_3^{0}$) as a function of pH at 150, 200 and 250 °C. The calculations are based on (a-c) the optimized thermodynamic data for La species (Table 5), and (d-f) Supcrt92 predictions. The calculated optimized pH values ($pH_{T,opt}$), La species molalities and La solubilities are listed in Table S2.

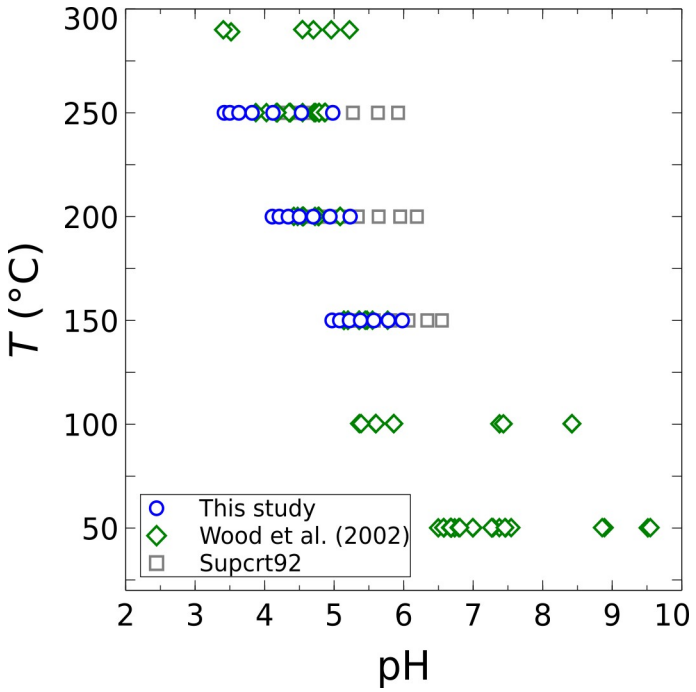

Fig. 8. Comparison of calculated pH as a function of temperature for the solubility of La hydroxide, showing that the optimized pH values are lower than predicted using Supcrt92. For comparison, the solubility data with in situ measured pH values are shown for Nd hydroxide from the study by Wood et al. (2002).

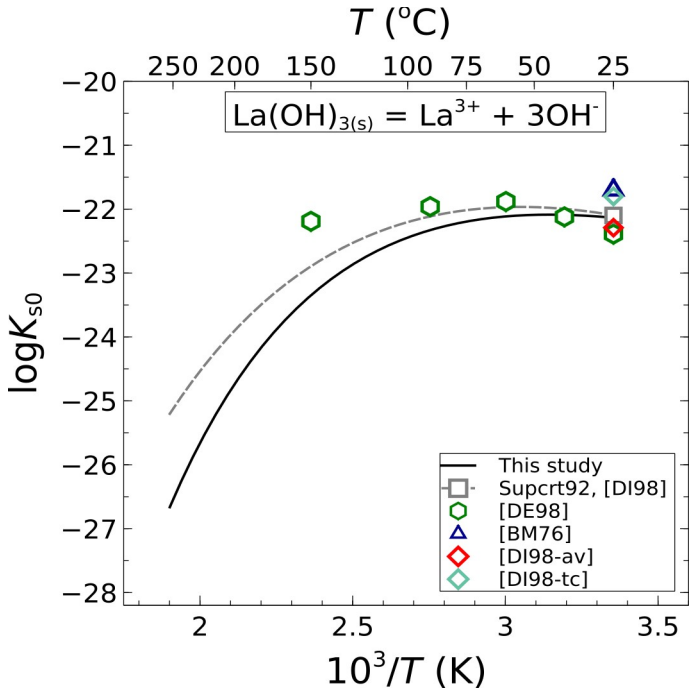

Fig. 9. Comparison of optimized La hydroxide solubility products (logK_{s0}) derived in this study (Table 7) with data derived from the literature. The grey dashed line was calculated using the thermodynamic properties of La^{3+} aqua ion from Supcrt92 and La hydroxide solid from Diakonov et al. (1998). Literature data: [DE98] Deberdt et al. (1998); [BM76] Baes and Mesmer (1976); [DI98] Diakonov et al. (1998), (av) averaged from the literature, (tc) based on thermochemical data. Literature data are listed in Table S3.

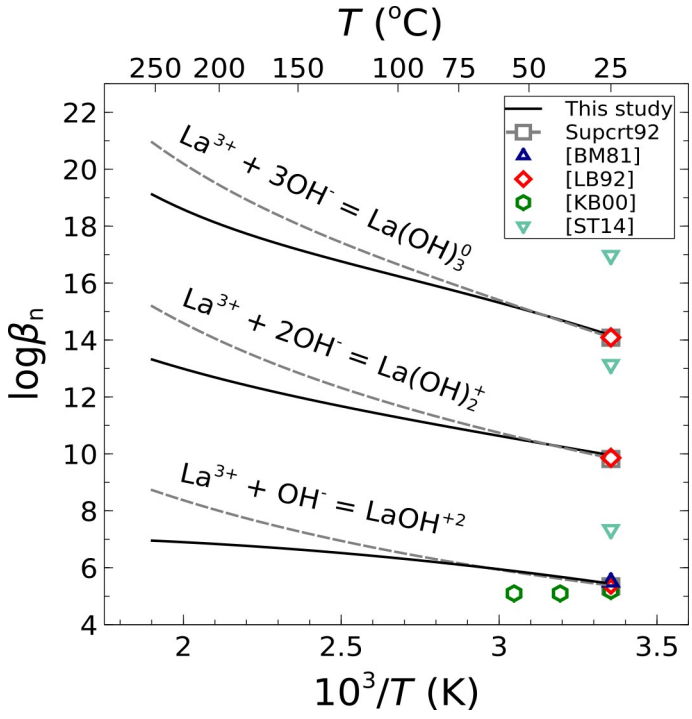

Fig. 10. Comparison of optimized formation constants for La hydroxyl complexes (logβ_n, n = 1 to 3) derived in this study (Table 7) with data derived from the literature. The grey dashed lines are calculated using the thermodynamic properties of La aqueous species from Supcrt92. Literature data at 25 °C: [BM81] Baes and Mesmer (1981); [LB92] Lee and Byrne (1992); [KB00] Klungness and Byrne (2000); [ST14] Stepanchikova et al. (2014). Literature data are listed in Table S4.

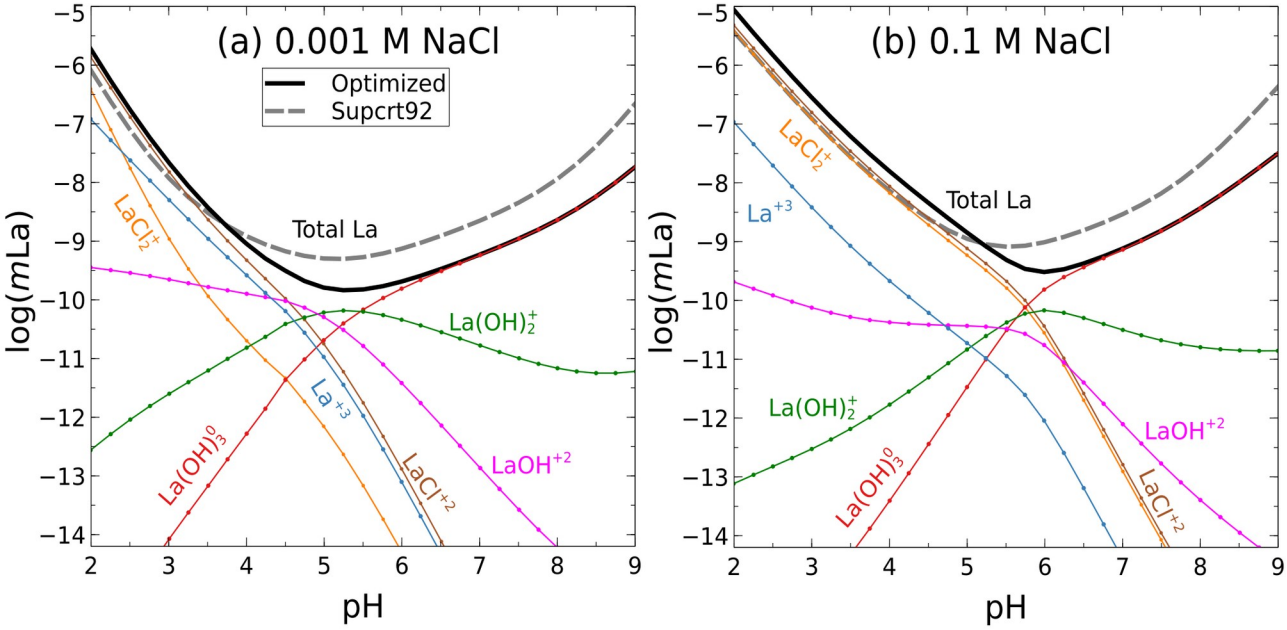

Fig. 11. Modeled monazite ($LaPO_4$) solubility and aqueous speciation as a function of pH and salinity at 250 °C using the thermodynamic properties of La aqueous species derived in this study. Total La concentrations calculated using Supcrt92 are shown for comparison. The model assumes the equilibration of $LaPO_4$ monazite with aqueous solutions containing 0.001 M NaCl (a) and 0.1 M NaCl (b); the pH was varied by adding HCl/NaOH. Thermodynamic properties for REE chloride complexes are from Migdisov et al. (2009) and were adjusted based on the properties of La^{3+} aqua ion derived in this study. Thermodynamic data for $LaPO_4$ are from Van Hoozen et al. (2020). Calculations were performed using GEMS (Kulik et al., 2013) and the MINES thermodynamic database (Gysi et al., 2023). The simulated speciation data are listed in Table S5.

TABLES

Table 1. Refined crystal unit cell parameters with the hexagonal structure ($P6_3/m$) for La hydroxide powders synthesized hydrothermally in this study and comparison with those reported in the literature.

a (Å)	*c* (Å)	Volume (Å^3)	Reference
6.542	3.862	143.136	This study
6.547	3.854	143.063	Beall et al. (1977)
6.520	3.844		Dordevic et al. (2014)
6.523	3.855		Roy and McKinstry (1953)

Table 2. Sources of thermodynamic data for La aqueous species and La hydroxide solid used for initial equilibrium calculations. The data for other species were not updated in this study.

Species	References
La- aqueous species	
La^{3+}	1, 2
$LaOH^{2+}$	3
$La(OH)_2^+$	3
$La(OH)_3^0$	3
$La(OH)_4^-$	3
Other species	
O_2^0, H_2^0	4
OH^-, H^+	1, 2
ClO_4^-	1, 2
La hydroxide solid	
$La(OH)_{3(s)}$	5, 6

[1]Shock et al. (1997); [2]Shock and Helgeson (1988); [3]Haas et al. (1995); [4]Shock et al. (1989); [5]Diakonov et al. (1998); [6]Navrotsky et al. (2015).

Table 3. Thermodynamic data for La hydroxide solid used for initial equilibrium calculations. The heat capacity function is described by: $C_P° = a + bT + c/T^2 + d/T$, where T is the temperature in Kelvin.

Variable	Units	Values	References
$\Delta_f G°_{Tr,\,Pr}$	kJ·mol^{-1}	-1284.2±1.3	1, 2
$\Delta_f H°_{Tr,\,Pr}$	kJ·mol^{-1}	-1416.1[4]	1, 2
$S°_{Tr,}$	J·mol^{-1}K^{-1}	117.81[5]	1, 2
$C_P°$	J·mol^{-1}K^{-1}	117.38[5]	1
a		174.60[5]	1
b		0.011336[5]	1
c		796395.62[5]	1
d		−20746.01[5]	1
Δa		8403.3	3
Δb		-17.184	3
$\Delta c \times 10^{-5}$		-3754.05	3

[1]Diakonov et al. (1998); [2]Navrotsky et al. (2015); [3]this study, where Δa-Δc indicate the heat capacity coefficients for the La hydroxide dissolution reaction, $La(OH)_3(s) = La^{3+} + 3OH^-$, derived from our solubility data and integration of the fitted solubility products using the the Van't Hoff relation $\partial \ln K / \partial T = \Delta H°_T / (RT)^2$ and Kirschoff's equation $[\partial \Delta H / \partial T]_P = \Delta C_P$; [4]based on enthalpy of solution for Ln (metal) and $La(OH)_{3(s)}$, average of the data of Cordfunke et al. (1990) and Merli et al. (1997); [5]based on adiabatic calorimetry data from Chirico and Westrum (1980).

Table 4. Starting pH, reaction times, and compositions (logarithm molality, mol/kg) of the quenched experimental solutions after equilibration with La hydroxide solids at temperatures of 150, 200, and 250 °C at saturated water vapor pressure.

Time (days)	Type[1]	*T* (°C)	$pH_{25°C,initial}$[2]	log(*m*ClO_4^-) (mol/kg)	log(*m*La) (mol/kg)
19	e	150	2.0	-1.95	-2.49
21	e	150	2.0	-1.95	-2.49
24	e	150	2.0	-1.95	-2.46
26	e	150	2.0	-1.95	-2.44
19	e	150	2.5	-2.47	-3.00
21	e	150	2.5	-2.47	-2.97
24	e	150	2.5	-2.47	-2.95
26	e	150	2.5	-2.47	-2.97
7	k	150	3.0	-2.98	-3.92
11	k	150	3.0	-2.98	-3.72
14	e	150	3.0	-2.98	-3.62
17	e	150	3.0	-2.98	-3.51
20	e	150	3.0	-2.98	-3.54
23	e	150	3.0	-2.98	-3.51
26	e	150	3.0	-2.98	-3.47
23	e	150	3.5	-3.49	-3.98
26	e	150	3.5	-3.49	-3.93
17	e	150	4.0	-4.00	-4.46
17	e	150	4.0	-4.00	-4.41
17	e	150	4.5	-4.50	-4.98
17	e	150	4.5	-4.50	-4.87
17	e	150	5.0	-5.00	-5.40
19	e	150	5.0	-5.00	-5.23
17	e	200	2.0	-1.95	-2.44
17	e	200	2.0	-1.95	-2.49
17	e	200	2.5	-2.47	-2.99
17	e	200	2.5	-2.47	-2.91
17	e	200	3.0	-2.98	-3.48
17	e	200	3.0	-2.98	-3.48
17	e	200	3.5	-3.49	-3.86
17	e	200	3.5	-3.49	-3.87
17	e	200	4.0	-4.00	-4.59
17	e	200	4.0	-4.00	-4.62
17	e	200	4.5	-4.50	-4.67
17	e	200	5.0	-5.00	-5.28
17	e	200	5.0	-5.00	-5.77
1	k	250	2.0	-1.95	-3.16
3	k	250	2.0	-1.95	-3.05
6	k	250	2.0	-1.95	-2.74
8	k	250	2.0	-1.95	-2.72
10	k	250	2.0	-1.95	-2.61

Table 4. (Continued)

Time (days)	Type[1]	*T* (°C)	$pH_{25°C,initial}$[2]	log(*m*ClO_4^-) (mol/kg)	log(*m*La) (mol/kg)
12	e	250	2.0	-1.95	-2.52
14	e	250	2.0	-1.95	-2.50
18	e	250	2.0	-1.95	-2.46
22	e	250	2.0	-1.95	-2.42
25	e	250	2.0	-1.95	-2.42
10	e	250	2.5	-2.47	-3.08
12	e	250	2.5	-2.47	-2.89
14	e	250	2.5	-2.47	-3.03
18	e	250	2.5	-2.47	-2.96
22	e	250	2.5	-2.47	-2.96
10	e	250	3.0	-2.98	-3.42
12	e	250	3.0	-2.98	-3.56
14	e	250	3.0	-2.98	-3.49
16	e	250	3.0	-2.98	-3.47
10	e	250	3.5	-3.49	-4.10
12	e	250	3.5	-3.49	-4.15
14	e	250	3.5	-3.49	-4.07
11	e	250	4.0	-4.00	-4.92
13	e	250	4.0	-4.00	-4.72
16	e	250	4.0	-4.00	-4.82
19	e	250	4.0	-4.00	-4.90
16	e	250	4.0	-4.00	-4.86
19	e	250	4.0	-4.00	-4.91
11	e	250	4.5	-4.50	-6.17
13	e	250	4.5	-4.50	-6.05
14	e	250	4.5	-4.50	-6.09
16	e	250	4.5	-4.50	-5.79
14	e	250	4.5	-4.50	-6.11
16	e	250	4.5	-4.50	-5.82
14	e	250	5.0	-5.00	-6.76
19	e	250	5.0	-5.00	-7.17

[1]Kinetic runs are identified by a “k” and equilibrium experiments by an “e”, respectively.

[2]Starting pH of the perchloric acid-based experimental buffer solutions at 25 °C and 1 bar before reaction with La hydroxide.

Table 5. Optimized **s**tandard partial molal Gibbs energy of formation at temperature *T* ($\Delta_f G°_T$) for La aqueous species and La hydroxide solid based on thermodynamic parameter optimizations using GEMSFITS and the solubility data from Table 4. The $\Delta_f G°_T$ values from Sucprt92 are also listed with references listed in Table 2.

	T=25 °C	*T*=100 °C[3]				*T*=150 °C				*T*=200 °C				*T*=250 °C			
Species	$\Delta_f G°_T$ (Supcrt92) kJ·mol^{-1}	$\Delta_f G°_T$ (Supcrt92) kJ·mol^{-1}	$\Delta_f G°_T$ (this study) kJ·mol^{-1}	Δ[1] kJ·mol^{-1}	Op[2]	$\Delta_f G°_T$ (Supcrt92) kJ·mol^{-1}	$\Delta_f G°_T$ (this study) kJ·mol^{-1}	Δ[1] kJ·mol^{-1}	Op[2]	$\Delta_f G°_T$ (Supcrt92) kJ·mol^{-1}	$\Delta_f G°_T$ (this study) kJ·mol^{-1}	Δ[1] kJ·mol^{-1}	Op[2]	$\Delta_f G°_T$ (Supcrt92) kJ·mol^{-1}	$\Delta_f G°_T$ (this study) kJ·mol^{-1}	Δ[1] kJ·mol^{-1}	Op[2]
La^{3+}	-686.17	-668.73	-665.79	2.94	O	-655.99	-656.83	-0.85	O	-642.23	-645.91	-3.68	O	-627.17	-633.63	-6.46	O
$LaOH^{2+}$	-874.04	-871.11	-868.16	2.94	R	-868.37	-862.33	6.04	O	-864.97	-858.19	6.79	O	-860.74	-850.13	10.61	O
$La(OH)_2^+$	-1056.83	-1063.51	-1060.57	2.94	R	-1066.87	-1057.23	9.65	O	-1069.56	-1061.99	7.57	O	-1071.57	-1059.93	11.65	O
$La(OH)_3^0$	-1238.42	-1254.41	-1251.47	2.94	R	-1262.68	-1252.71	9.97	R	-1269.54	-1261.97	7.57	R	-1275.20	-1263.56	11.65	R
$La(OH)_{3(s)}$	-1284.20	-	-		-	-1301.77	-1304.68	-2.90	O	-1310.22	-1321.39	-11.18	O	-1319.34	-1338.51	-19.16	O

Op: Optimization; O: Optimized; R: Reaction constrained.

[1]Difference $\Delta_f G°_T$(this study) - $\Delta_f G°_T$(Supcrt92).

[2]Selected species that were poorly constrained in the studied experimental pH range were reaction constrained using the equilibrium constants listed by Haas et at. (1995) according to Eqs. 4-6.

[3]Optimizations based on the $LaPO_4$ solubility data at pH 2 by Van Hoozen et al. (2020).

Table 6. Regressed coefficients and R^2 for fits of the temperature dependence (between 25 and 250 °C) of the standard partial molal Gibbs energy of formation ($\Delta_f G°_T$ in J/mol) of aqueous La species optimized in this study (Table 5). The fits are described by $\Delta_f G°_T = a + bT + c/T$, with T in Kelvin.

Species	$a\times10^{-3}$	b	$c\times10^{-4}$	R^2
La^{3+}	-716.4	182.8	-712.1	0.997
$LaOH^{2+}$	-960.2	171.0	1049.9	0.994
$La(OH)_2^+$	-1079.0	17.3	499.9	0.375
$La(OH)_3^0$	-1281.6	-19.5	1453.1	0.965

Table 7. Regressed coefficients for the function expressing the logarithm of the solubility product ($\log K_{s0}$) of La hydroxide (Eq. 3) and the hydrolysis constants ($\log\beta_{1-3}$) for La hydroxyl species (Eq. 4-6) as a function of temperature from 25 to 250 °C. These regressions are generated using the optimized thermodynamic properties for La aqueous species and La hydroxide derived in this study (Table 5), and the properties of OH^- from Shock et al. (1997) and Shock and Helgeson (1988). The logarithm of the equilibrium constants ($\log K$, where $\log K$ stands for $\log K_{s0}$ and $\log\beta_{1-3}$) are expressed as a function of temperature: $\log K = A_0 + A_1 T + A_2/T + A_3 \ln T + A_4/T^2$, with T in Kelvin.

Reactions		$\log K$ (25 °C, 1 bar)	A_0	A_1	$A_2\times10^{-3}$	A_3	$A_4\times10^{-4}$
$La(OH)_{3(s)} = La^{3+} + 3OH^-$	(K_{s0})	-22.2	-2801	-0.449	155.8	438.9	-980.4
$La^{3+} + OH^- = LaOH^{2+}$	(β_1)	5.4	937	0.137	-49.8	-146.3	247.2
$La^{3+} + 2OH^- = La(OH)_2^+$	(β_2)	9.9	1882	0.274	-106.1	-292.6	615.1
$La^{3+} + 3OH^- = La(OH)_3^0$	(β_3)	14.2	2821	0.411	-158.1	-438.9	904.5

Table 8. Comparison between predicted (Haas et al., 1995) and experimentally derived formation constants for La hydrolysis (this study, Table 7) and for Nd hydrolysis (Wood et al., 2002).

T	La hydrolysis		Nd hydrolysis	
	[1]This		[3]Wood et al.	
(°C)	study	[2]Supcrt92	(2002)	[4]Supcrt92
	$\log\beta_1$: $REE^{3+} + OH^- = REEOH^{2+}$			
250	7.0	8.7	7.4	9.2
290	7.2	9.4	8.0	9.8
	$\log\beta_2$: $REE^{3+} + 2OH^- = REE(OH)_2^+$			
250	13.3	15.2		
290	14.0	16.3	14.1	17.1
	$\log\beta_3$: $REE^{3+} + 3OH^- = REE(OH)_3^0$			
250	19.1	20.9		
290	20.1	22.3	19.9	23.2

[1]Experimental values for La; [2]predicted values for La; [3]experimental values for Nd; [4]predicted values for Nd.

SUPPLEMENTARY MATERIAL

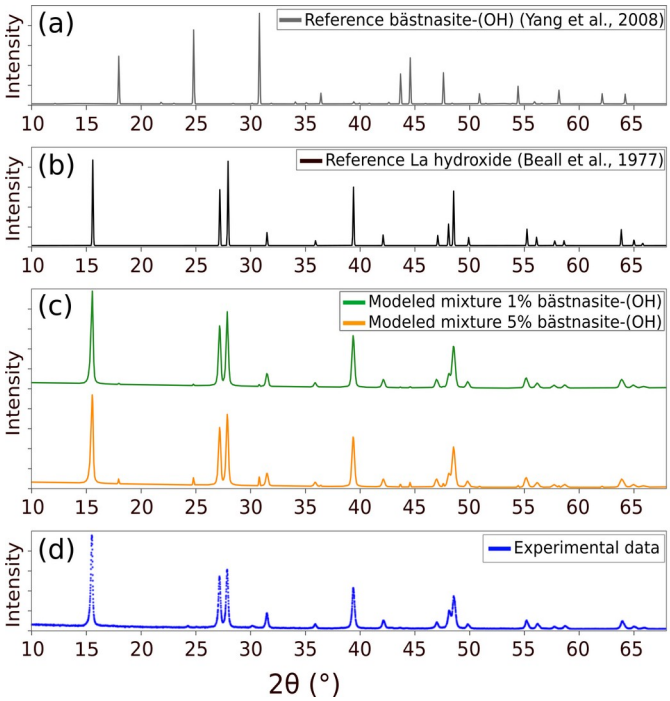

Fig S1. Comparison of X-ray diffractograms for (a) reference pattern of bastnäsite-(OH) with the structural formula $Ce_{0.50}Nd_{0.24}La_{0.23}Y_{0.03}CO_3[(OH)_{0.65}F_{0.35}]$ (Yang et al., 2008), (b) reference pattern of La hydroxide (Beall et al., 1977), (c) modeled mixtures containing 1% bastnäsite-(OH) + 99% La hydroxide (green), or 5% bastnäsite-(OH) + 95% La hydroxide (orange), and (d) La hydroxide powders synthesized in this study. The experimental spectra is comparable to that of the 1% bastnäsite-(OH) model, whereas the 5% bastnäsite-(OH) model shows peaks at ~18, 24.5 and 31 degrees 2θ with significantly higher intensities.

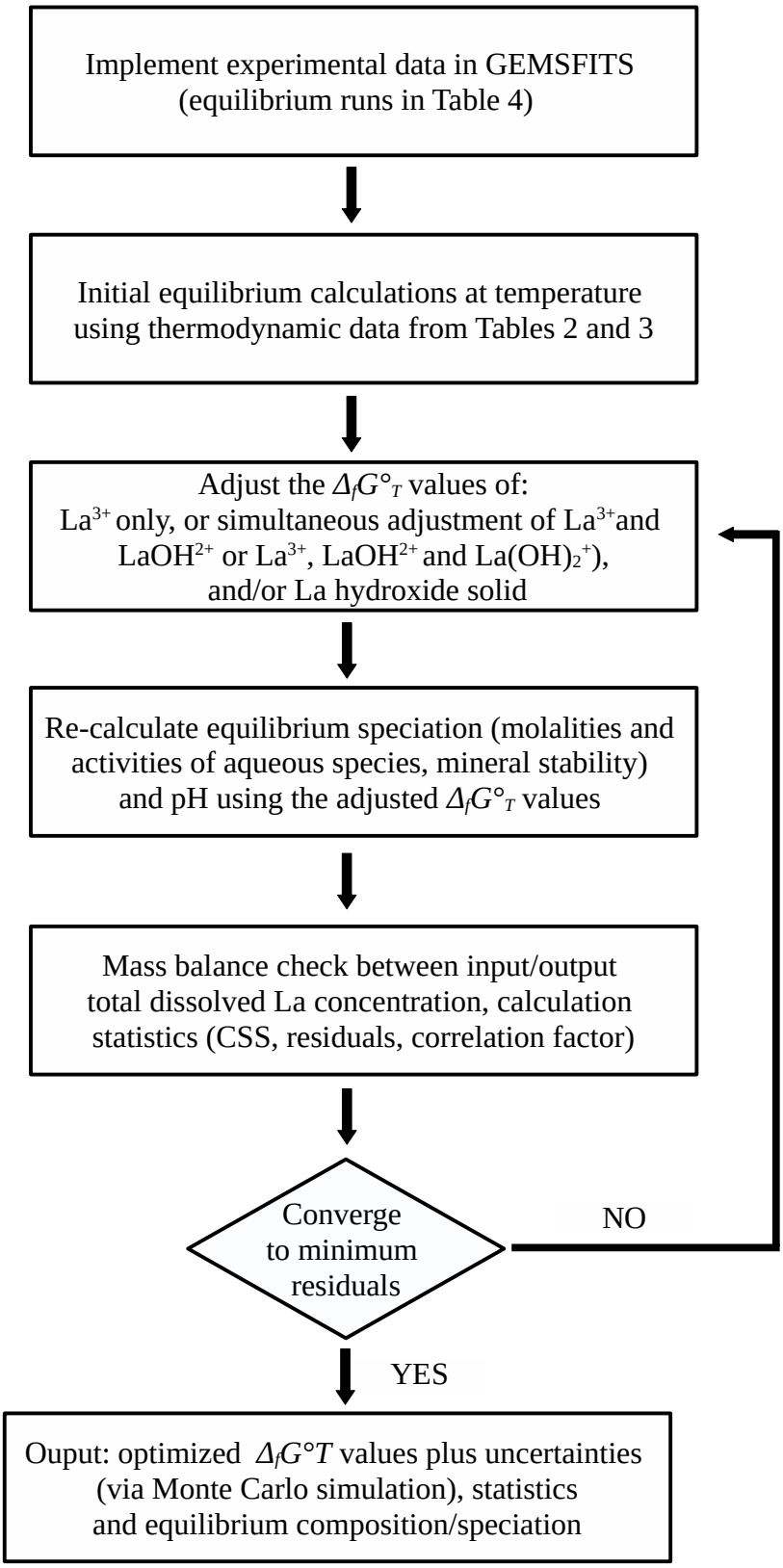

Fig. S2. Workflow chart of the parameter optimization using the GEMSFITS code package (Miron et al., 2015) coupled with GEMS3K chemical equilibrium solver (Kulik et al., 2013).

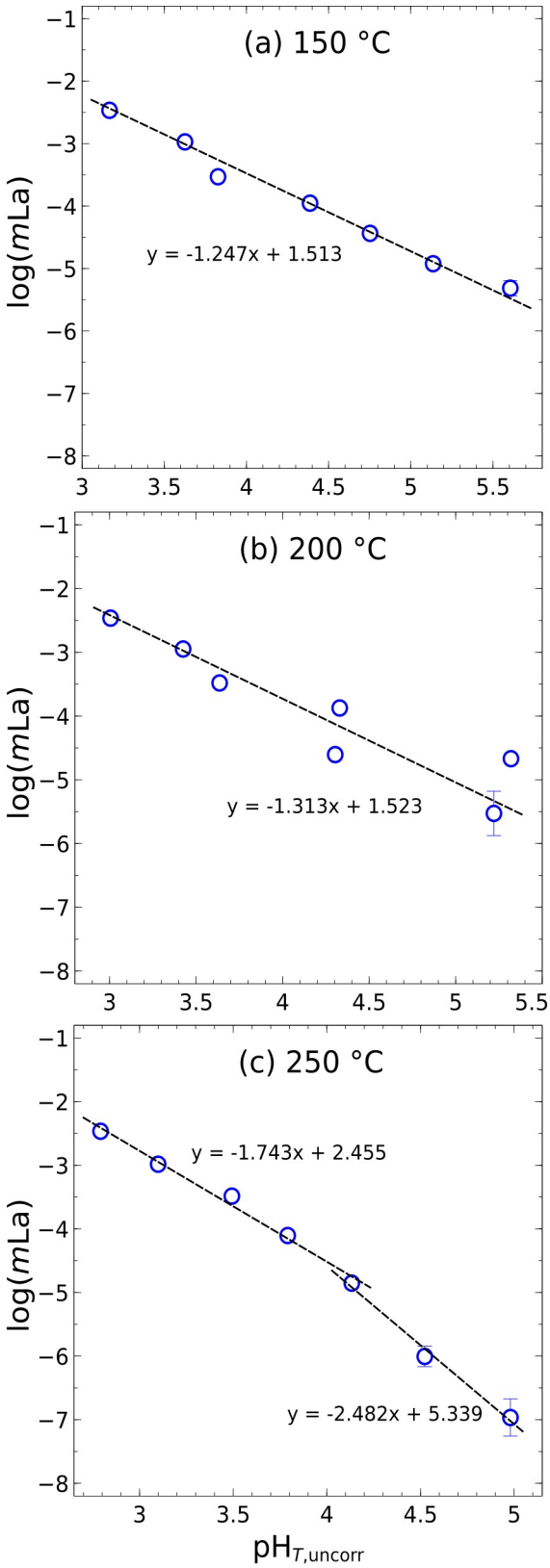

Fig. S3. Logarithm molality (mol/kg) of total dissolved La concentrations measured in the quenched experimental solutions as a function of pH, uncorrected and calculated *a priori* at the experimental temperature ($pH_{T,uncorr}$) at (a) 150, (b) 200 and (c) 250 °C using the thermodynamic properties for La aqueous species from Supcrt92 (Table 2). The solubility-$pH_{T,uncorr}$ profiles display slopes that are inconsistent with the stoichiometry of La hydroxide dissolution and La hydrolysis reactions (Eqs. 3-6). The calculated pH data are listed in Table S1.

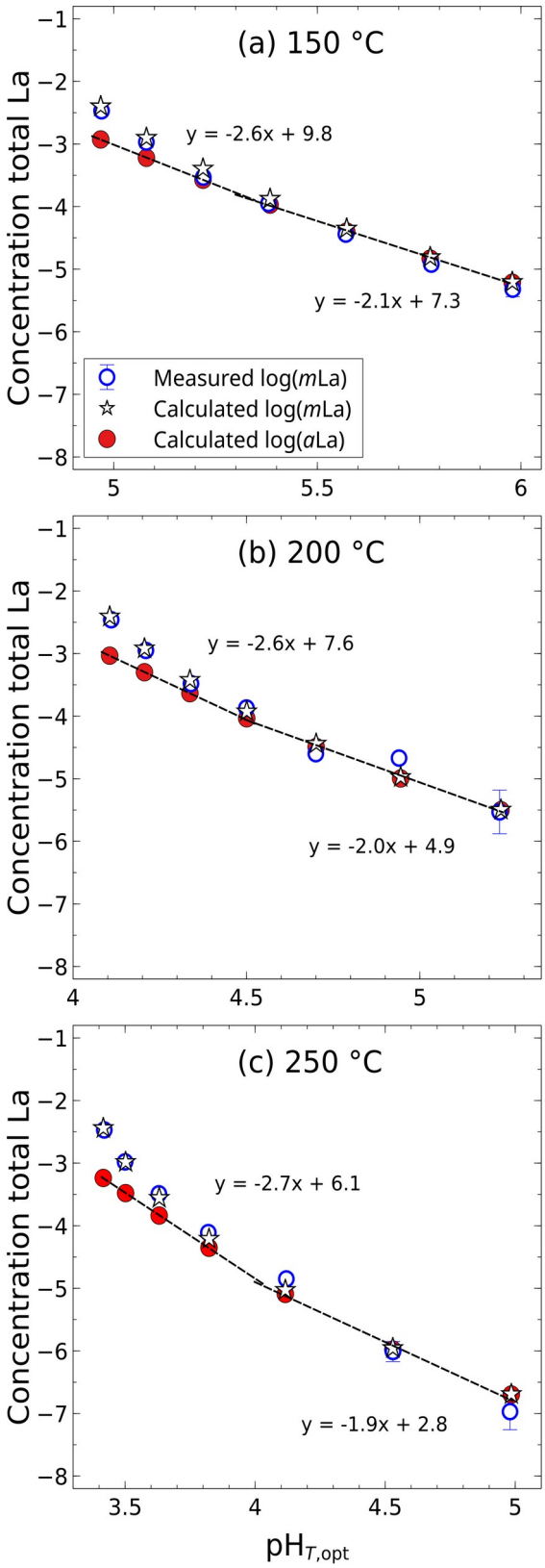

Fig. S4. Logarithm molality (mol/kg) and logarithm activity of total dissolved La in the quenched experimental solutions as a function of pH at (a) 150, (b) 200 and (c) 250 °C. The log activity of total La is calculated as the sum of activities of all dissolved La aqueous species and fitted to linear curves. The slopes of the curves have values that are different compared to those obtained when plotting log*m* of total La (Fig. 5) due to the effect of the activity coefficients, however, these slope values can be approximated to the theoretical values of -3 and -2, which are related to the La^{3+} and $LaOH^{+2}$, respectively. The theoretical slopes can be retrieved by using calculated aqueous La species activities. A slope of -2.7 to -2.6 indicates the presence of mainly La^{3+} and lesser $LaOH^{2+}$. A

slope of -1.9 to -2.1 indicates the presence of mainly $LaOH^{2+}$.

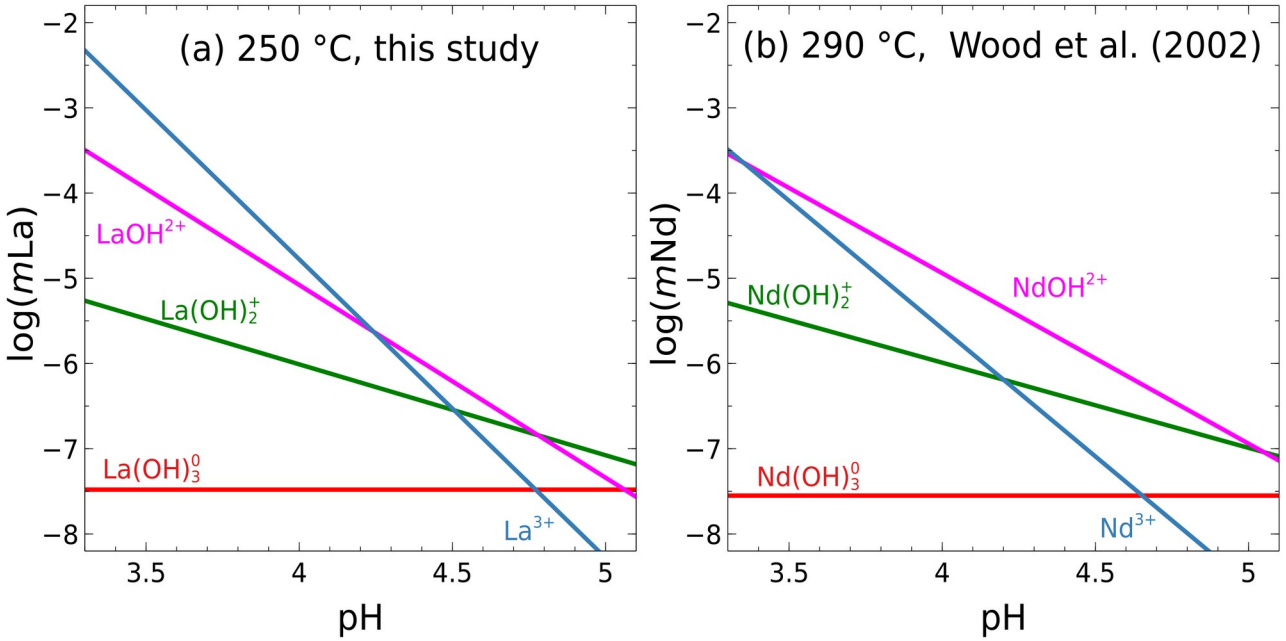

Fig S5. Calculated logarithm molality (in mol/kg) of (a) total dissolved La concentrations and La aqueous species (La^{3+}, $LaOH^{2+}$, $La(OH)_2^+$ and $La(OH)_3^0$) as a function of pH at 250 °C from this study and (b) total dissolved Nd concentrations and Nd aqueous species (Nd^{3+}, $NdOH^{2+}$, $Nd(OH)_2^+$ and $Nd(OH)_3^0$) as a function of pH at 290 °C (modified from Wood et al., 2002). Both experimental speciation models indicate that the REE^{3+} aqua ion predominates over the hydroxyl complexes at acidic pH below ~3.3, whereas at pH higher than 4.5 the $REEOH^{2+}$, $REE(OH)_2^+$ complexes predominates over the REE^{3+} aqua ion.

Table S1. Equilibrium speciation of experimental solutions equilibrated with La hydroxide solids at temperatures of 150 to 250 °C calculated using GEMS (Kulik et al., 2013) and the thermodynamic properties of La aqueous species compiled in Supcrt92 (Table 2). The calculated and uncorrected equilibrium pH values ($pH_{T,uncorr}$) result in solubility-$pH_{T,uncorr}$ profiles inconsistent with the stepwise hydrolysis of ions with pH (Fig. S3) due to inaccurate estimations of the stability of La aqueous species using Supcrt92.

T (°C)	$pH_{T,\ uncorr}$	log(*m*La) measured	log*m*La^{3+}	log*m*$LaOH^{2+}$	log*m*$La(OH)_2^{+}$	log*m*$La(OH)_3^{0}$	log*m*$La(OH)_4^{-}$
150	3.2	-2.5	-2.5	-4.1	-7.2	-10.6	-16.9
150	3.6	-3.0	-3.0	-4.0	-6.6	-9.4	-15.3
150	3.8	-3.5	-3.6	-4.3	-6.7	-9.4	-15.2
150	4.4	-4.0	-4.2	-4.3	-6.0	-8.0	-13.2
150	4.8	-4.4	-5.0	-4.6	-6.0	-7.6	-12.4
150	5.1	-4.9	-5.8	-5.0	-6.0	-7.3	-11.7
150	5.6	-5.3	-6.7	-5.5	-6.0	-6.8	-10.7
200	3.0	-2.5	-2.5	-3.3	-5.9	-8.8	-14.4
200	3.4	-3.0	-3.2	-3.3	-5.4	-7.8	-13.1
200	3.6	-3.5	-3.9	-3.7	-5.5	-7.7	-12.8
200	4.3	-3.9	-4.9	-4.0	-5.0	-6.5	-10.9
200	4.3	-4.6	-5.6	-4.7	-5.7	-7.2	-11.7
200	5.3	-4.7	-7.0	-5.0	-5.0	-5.5	-9.0
200	5.2	-5.5	-7.7	-5.8	-5.9	-6.5	-10.0
250	2.8	-2.5	-2.7	-2.9	-5.2	-7.9	-13.1
250	3.1	-3.0	-3.5	-3.2	-5.0	-7.4	-12.3
250	3.5	-3.5	-4.4	-3.6	-4.9	-6.9	-11.4
250	3.8	-4.1	-5.4	-4.2	-5.2	-6.8	-11.1
250	4.1	-4.9	-6.6	-5.0	-5.6	-6.9	-10.8
250	4.5	-6.0	-8.3	-6.2	-6.5	-7.4	-10.9
250	5.0	-7.0	-10.0	-7.5	-7.2	-7.7	-10.8

Table S2. Aqueous speciation calculations using GEMS and the optimized La species properties from Table 5. Listed are the optimized pH values ($pH_{T,opt}$), the total dissolved La molalities (mLa) and aqueous La species molalities for experimental solutions equilibrated with La hydroxide solids at temperatures of 150, 200, and 250 °C at saturated water vapor pressure.

T (°C)	$pH_{T,opt}$	log(mLa)[1] measured	σ[1]	log(mLa) calculated	log$m$La^{3+}	log$m$LaOH^{2+}	log$m$La(OH)$_2^+$	log$m$La(OH)$_3^0$
150	5.0	-2.5	0.03	-2.4	-2.5	-3.1	-4.9	-6.4
150	5.1	-3.0	0.02	-2.9	-3.1	-3.4	-5.0	-6.4
150	5.2	-3.5	0.05	-3.4	-3.6	-3.8	-5.2	-6.4
150	5.4	-4.0	0.04	-3.9	-4.2	-4.2	-5.3	-6.4
150	5.6	-4.4	0.04	-4.4	-4.9	-4.6	-5.5	-6.4
150	5.8	-4.9	0.08	-4.8	-5.5	-5.0	-5.7	-6.4
150	6.0	-5.3	0.12	-5.2	-6.1	-5.4	-5.9	-6.4
200	4.1	-2.5	0.04	-2.4	-2.5	-3.2	-4.8	-6.6
200	4.2	-2.9	0.06	-2.9	-3.0	-3.5	-4.9	-6.6
200	4.3	-3.5	0.00	-3.4	-3.6	-3.9	-5.0	-6.6
200	4.5	-3.9	0.01	-3.9	-4.2	-4.3	-5.2	-6.6
200	4.7	-4.6	0.02	-4.4	-4.9	-4.7	-5.4	-6.6
200	4.9	-4.7	0.00	-5.0	-5.7	-5.2	-5.7	-6.6
200	5.2	-5.5	0.35	-5.5	-6.6	-5.8	-6.0	-6.6
250	3.4	-2.5	0.04	-2.4	-2.5	-3.6	-5.3	-7.5
250	3.5	-3.0	0.07	-3.0	-3.0	-4.0	-5.5	-7.5
250	3.6	-3.5	0.06	-3.6	-3.6	-4.3	-5.6	-7.5
250	3.8	-4.1	0.04	-4.2	-4.4	-4.8	-5.8	-7.5
250	4.1	-4.9	0.07	-5.0	-5.3	-5.4	-6.1	-7.5
250	4.5	-6.0	0.16	-6.0	-6.6	-6.3	-6.6	-7.5
250	5.0	-7.0	0.29	-6.7	-8.0	-7.2	-7.0	-7.5

[1]Mean values and the standard deviation (σ) of the mean are calculated from replicate experimental data in Table 4.

Table S3. Optimized La hydroxide solubility products (logK_{s0}) calculated using the regressed coefficients in Table 7 and comparison with literature data.

T (°C)	logK_{s0}: La(OH)$_{3(s)}$ = La^{3+} + 3OH$^-$ 1	2	3	4	5	6
25	-22.2	-22.1	-22.4	-21.7	-22.3	-21.8
40	-22.1	-22.0	-22.1			
60	-22.1	-22.0	-21.9			
90	-22.3	-22.1	-22.0			
150	-23.4	-22.9	-22.2			
200	-24.7	-23.9				
250	-26.6	-25.3				

[1]This study; [2]Supcrt92 and La hydroxide solid from Diakonov et al. (1998); [3]Deberdt et al. (1998); [4]Baes and Mesmer (1976); [5]Diakonov et al. (1998), averaged from the literature; [6]Diakonov et al. (1998), based on thermochemical data.

Table S4. Optimized formation constants for La hydroxyl complexes ($\log\beta_{1\text{-}3}$) calculated using the regressed coefficients in Table 7 and comparison with literature data.

T	References					
(°C)	1	2	3	4	5	6
	$\log\beta_1$: $La^{3+} + OH^- = LaOH^{2+}$					
25	5.4	5.4	5.2	5.3	7.3	5.5
40	5.7	5.6	5.1			
55	5.9	5.9	5.1			
150	6.6	7.3				
200	6.8	8.0				
250	7.0	8.7				
	$\log\beta_2$: $La^{3+} + 2OH^- = La(OH)_2^+$					
25	9.9	9.8		9.9	13.1	
150	12.0	12.8				
200	12.6	14.0				
250	13.3	15.2				
	$\log\beta_3$: $La^{3+} + 3OH^- = La(OH)_3^0$					
25	14.2	14.1		14.1	17.0	
150	17.2	18.1				
200	18.1	19.4				
250	19.1	20.9				

[1]This study; [2]Supcrt92; [3]Klungness and Byrne (2000); [4]Lee and Byrne (1992); [5]Stepanchikova et al. (2014); [6]Baes and Mesmer (1981).

Table S5. Calculated logarithm molality ($\log m$) of total dissolved La and aqueous species in aqueous hydrothermal solutions with salinity of 0.01 and 0.1 M NaCl and pH of 2-9 in equilibrium with monazite ($LaPO_4$) at 250 °C. The calculations were performed using the thermodynamic properties of La aqueous species derived in this study (Table 5). Thermodynamic data for REE chloride complexes are from Migdisov et al. (2009), which were adjusted based on La^{3+} from this study, and those of $LaPO_4$ are from Van Hoozen et al. (2020). Calculated values below -14.0 are omitted.

Salinity M NaCl	pH	Total La $\log m$	La^{+3} $\log m$	$LaOH^{+2}$ $\log m$	$La(OH)_2^+$ $\log m$	$La(OH)_3^0$ $\log m$	$LaCl^{+2}$ $\log m$	$LaCl_2^+$ $\log m$
0.001	2.0	-5.7	-6.9	-9.4	-12.6	-	-5.9	-6.4
	3.0	-7.7	-8.3	-9.7	-11.6	-	-7.8	-9.0
	4.0	-9.0	-9.6	-9.9	-10.8	-12.3	-9.3	-10.7
	5.0	-9.8	-11	-10.3	-10.2	-10.7	-10.7	-12.2
	6.0	-9.7	-13.1	-11.4	-10.3	-9.8	-12.9	-
	7.0	-9.2	-	-12.9	-10.8	-9.2	-	-
	8.0	-8.6	-	-	-11.2	-8.6	-	-
	9.0	-7.7	-	-	-11.2	-7.7	-	-
0.1	2.0	-5.1	-7.0	-9.7	-13.1	-	-5.3	-5.4
	3.0	-6.5	-8.4	-10.1	-12.5	-	-6.8	-6.9
	4.0	-7.8	-9.7	-10.4	-11.8	-13.4	-8.1	-8.2
	5.0	-8.8	-10.7	-10.4	-10.8	-11.5	-9.1	-9.2
	6.0	-9.5	-12.0	-10.8	-10.2	-9.8	-10.4	-10.5
	7.0	-9.1	-	-12.1	-10.5	-9.1	-12.8	-12.9
	8.0	-8.4	-	-13.4	-10.8	-8.4	-	-
	9.0	-7.5	-	-	-10.9	-7.5	-	-

REFERENCES

Yang H., Dembowski R. F., Conrad P. G. and Downs R. T. (2008) Crystal structure and Raman spectrum of hydroxyl-bästnasite-(Ce), $CeCO_3(OH)$. American Mineralogist 93, 698–701.